NASA/TM–2003-212268

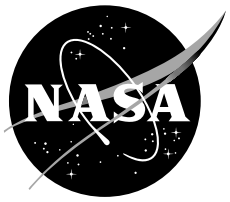

Direct Validation of the Wall Interference Correction System of the Ames 11-Foot Transonic Wind Tunnel

Norbert Ulbrich and Alan R. Boone

May 2003

The NASA STI Program Office . . . in Profile

Since its founding, NASA has been dedicated to the advancement of aeronautics and space science. The NASA Scientific and Technical Information (STI) Program Office plays a key part in helping NASA maintain this important role.

The NASA STI Program Office is operated by Langley Research Center, the Lead Center for NASA's scientific and technical information. The NASA STI Program Office provides access to the NASA STI Database, the largest collection of aeronautical and space science STI in the world. The Program Office is also NASA's institutional mechanism for disseminating the results of its research and development activities. These results are published by NASA in the NASA STI Report Series, which includes the following report types:

- TECHNICAL PUBLICATION. Reports of completed research or a major significant phase of research that present the results of NASA programs and include extensive data or theoretical analysis. Includes compilations of significant scientific and technical data and information deemed to be of continuing reference value. NASA's counterpart of peer-reviewed formal professional papers but has less stringent limitations on manuscript length and extent of graphic presentations.

- TECHNICAL MEMORANDUM. Scientific and technical findings that are preliminary or of specialized interest, e.g., quick release reports, working papers, and bibliographies that contain minimal annotation. Does not contain extensive analysis.

- CONTRACTOR REPORT. Scientific and technical findings by NASA-sponsored contractors and grantees.

- CONFERENCE PUBLICATION. Collected papers from scientific and technical conferences, symposia, seminars, or other meetings sponsored or cosponsored by NASA.

- SPECIAL PUBLICATION. Scientific, technical, or historical information from NASA programs, projects, and missions, often concerned with subjects having substantial public interest.

- TECHNICAL TRANSLATION. English-language translations of foreign scientific and technical material pertinent to NASA's mission.

Specialized services that complement the STI Program Office's diverse offerings include creating custom thesauri, building customized databases, organizing and publishing research results . . . even providing videos.

For more information about the NASA STI Program Office, see the following:

- Access the NASA STI Program Home Page at *http://www.sti.nasa.gov*

- E-mail your question via the Internet to help@sti.nasa.gov

- Fax your question to the NASA Access Help Desk at (301) 621-0134

- Telephone the NASA Access Help Desk at (301) 621-0390

- Write to:
  NASA Access Help Desk
  NASA Center for AeroSpace Information
  7121 Standard Drive
  Hanover, MD 21076-1320

NASA/TM–2003-212268

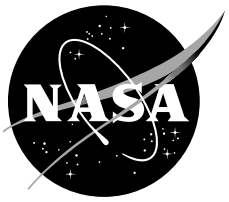

Direct Validation of the Wall Interference Correction System of the Ames 11-Foot Transonic Wind Tunnel

Norbert Ulbrich
Sverdrup Technology, Inc., P.O. Box 366, Moffett Field, California

Alan R. Boone
Ames Research Center, Wind Tunnel Operations Division, Moffett Field, California

National Aeronautics and
Space Administration

Ames Research Center
Moffett Field, California 94035-1000

May 2003

Acknowledgments

We want to thank the management and staff of the Wind Tunnel Operations Division at Ames Research Center for their support. The successful planning and completion of the validation test would have been impossible without their contributions. We would also like to thank The Boeing Company who generously allowed us to use one of their semispan wind tunnel models for the validation test.

Available from:

NASA Center for AeroSpace Information
7121 Standard Drive
Hanover, MD 21076-1320
(301) 621-0390

National Technical Information Service
5285 Port Royal Road
Springfield, VA 22161
(703) 487-4650

PREFACE

During the past two years, substantial progress was made in the development of TWICS, the real–time wall interference corrections system of the Ames 11–Foot Transonic Wind Tunnel. All initial system performance and reliability goals were met. In addition, computed corrections showed good agreement with corrections that were determined using alternate correction methods.

A direct validation of TWICS, i.e., a comparison of sets of corrected aerodynamic coefficients, was still needed in order to study the absolute accuracy of the correction system over the whole angle of attack and subsonic Mach number range. Finally, in the summer of 2002 experimental data from the test of a large semispan model became available that could be used to perform this direct validation. Results of the validation test are discussed in the present report.

We hope that experiences made during the successful direct validation of TWICS will benefit future efforts to develop real–time wall interference correction systems for transonic wind tunnels. These correction systems will eventually make it possible to record test data at constant corrected Mach number.

We want to thank the management and staff of the Wind Tunnel Operations Division at Ames Research Center for their support. The successful planning and completion of the validation test would have been impossible without their contributions. We also like to thank The Boeing Company who generously allowed us to use one of their semispan wind tunnel models for the validation test.

Moffett Field, California
May 2003

Norbert Ulbrich
Alan R. Boone

ABSTRACT

Data from the test of a large semispan model was used to perform a direct validation of a wall interference correction system for a transonic slotted wall wind tunnel. At first, different sets of uncorrected aerodynamic coefficients were generated by physically changing the boundary condition of the test section walls. Then, wall interference corrections were computed and applied to all data points. Finally, an interpolation of the corrected aerodynamic coefficients was performed. This interpolation made sure that the corrected Mach number of a given run would be constant. Overall, the agreement between corresponding interpolated lift, drag, and pitching moment coefficient sets was very good. Buoyancy corrections were also investigated. These studies showed that the accuracy goal of one drag count may only be achieved if reliable estimates of the wall interference induced buoyancy correction are available during a test.

TABLE OF CONTENTS

LIST OF SYMBOLS

A	cross–sectional area distribution of test article
b_δ	blockage part of wall signature
$b_{\delta,F}$	fitted wall signature
$b_{\delta,L}$	lifting part of wall signature
$b_{\delta,M}$	measured wall signature
c	reference chord *or* parabola coefficient
c_ξ	corrected aerodynamic coefficient
$\overline{c_\xi}$	aerodynamic coefficient after angle of attack interpolation
$\widehat{c_\xi}$	aerodynamic coefficient after Mach number interpolation
$\delta\widehat{c_\xi}$	difference of interpolated aerodynamic coefficients
c_D	corrected drag coefficient
c'_D	uncorrected drag coefficient
δc_D	difference of corrected drag coefficients
$\delta c'_D$	difference of uncorrected drag coefficients
Δc_D	total drag coefficient correction; $c_D - c'_D$
Δc_{D_2}	drag coefficient correction due to clear tunnel buoyancy
Δc_{D_3}	drag coefficient correction due to wall interference induced buoyancy
c_L	corrected lift coefficient
c'_L	uncorrected lift coefficient
δc_L	difference of corrected lift coefficients
$\delta c'_L$	difference of uncorrected lift coefficients
Δc_L	total lift coefficient correction; $c_L - c'_L$
c_M	corrected pitching moment coefficient
c'_M	uncorrected pitching moment coefficient
δc_M	difference of corrected pitching moment coefficients
$\delta c'_M$	difference of uncorrected pitching moment coefficients
Δc_M	total pitching moment coefficient correction; $c_M - c'_M$
Δc_{M1}	pitching moment coefficient correction due to the difference between mean and local angle of attack correction along the span of the wing

Δc_{M2}	pitching moment coefficient correction due to streamline curvature
c_p	pressure coefficient
D	corrected drag force
D'	uncorrected drag force
ΔD_1	drag force correction due to force inclination at 1/4 chord line
ΔD_2	drag force correction due to clear tunnel buoyancy
ΔD_3	drag force correction due to wall interference induced buoyancy
k	singularity index
L	corrected lift force
L'	uncorrected lift force
ΔL	lift force correction due to force inclination at 1/4 chord line
M	corrected Mach number
M'	uncorrected Mach number
$\overline{M}$	interpolated Mach number
m	total number of wall pressure ports
n	total number of test article singularities
P	corrected pitching moment
P'	uncorrected pitching moment
p_c	static pressure at a wall pressure port during empty tunnel calibration
p_t	static pressure at a wall pressure port during wind tunnel test
p_T	total pressure
q	corrected dynamic pressure
q'	uncorrected dynamic pressure
R	gas constant
S	test article reference area
T_T	total temperature
U_c	flow velocity at a wall pressure port during empty tunnel calibration
U_t	flow velocity at a wall pressure port during wind tunnel test
U'	uncorrected free–stream velocity (test section reference velocity)
$\overline{u_i}$	dimensionless perturbation velocity of wall interference flow field divided by singularity strength (x–component)

$\overline{u_t}$	dimensionless perturbation velocity of wind tunnel flow field divided by singularity strength (x–component)
Δu	axial perturbation velocity caused by wall interference effects
w	weighting factor of singularity
ω	weighting factor of reference point
V	test article volume
$\overline{v_i}$	dimensionless perturbation velocity of wall interference flow field divided by singularity strength (y–component)
Δv	perturbation velocity caused by wall interference effects (y–direction)
x	streamwise coordinate
y	y–coordinate
z	z–coordinate
α	corrected angle of attack
α'	uncorrected angle of attack
α_i	angle of attack correction at test article reference point
$\Delta\alpha_{0.25}$	averaged angle of attack correction along the 1/4 chord line
$\Delta\alpha_{0.75}$	averaged angle of attack correction along the 3/4 chord line
γ	isentropic exponent
δ	wall pressure port index
ε	blockage factor at reference point
$\overline{\varepsilon}$	averaged blockage factor
ζ	run index
η	total number of line doublets modeling lifting effects
λ	total number of reference points along 1/4 chord line
μ	total number of reference points along 3/4 chord line
ν	reference point index
ξ	total number of line doublets modeling lifting effects and point doublets modeling solid volume blockage *or* index of aerodynamic coefficient
σ	singularity strength

$\mathbf{A}$	matrix containing perturbation velocities of the wind tunnel flow field
$\mathbf{B}$	vector containing perturbation velocities caused by blockage effects
$\mathbf{X}$	vector containing singularity strength values

INTRODUCTION

During the past two years a system was developed for the Ames 11–Foot Transonic Wind Tunnel (TWT) that uses wall pressure measurements to estimate wind tunnel wall interference corrections. The system is called TWICS[1] (Transonic Wall Interference Correction System) and is based on the correction system WICS[2,3] (Wall Interference Correction System) that was originally developed for the Ames 12–Foot Pressure Wind Tunnel.

TWICS, similar to WICS, uses a highly modified version of the wall signature method to estimate wall interference corrections in real–time. Corrections are computed by combining a singularity representation of the test article and panel method code solutions of the wind tunnel and wall interference flow field with lift force, pitching moment, and wall pressure measurements. Lift force and pitching moment measurements are used to determine the strength of singularities representing lifting effects of the test article. A global least squares fit of the wall pressure signature is used to compute the strength of singularities that represent blockage effects of the test article. All initial system performance and reliability goals were met during the development of TWICS. The system is presently capable of computing corrections at a rate of 1 Hz.

So far, due to the complexity of the wall boundary condition of the slotted wall test section of the 11–Foot TWT, only a limited amount of data was available to study the absolute accuracy of wall interference corrections that TWICS computes. Whenever possible, computed corrections were compared with results that were determined using alternate correction methods. The angle of attack correction showed excellent agreement during these investigations. A validation of the blockage correction was more difficult as alternate correction methods selected for the comparison did not use wall pressure measurements. The blockage correction showed good agreement at zero lift where a comparison between TWICS and alternate methods was possible. However, no comparison of the blockage correction at higher angles of attack could be performed.

The validation of a wall interference correction system requires more than just a comparison of corrections that are derived from different methods. Each method is usually based on a simplifying description of the wind tunnel and wall interference flow field and therefore contains modeling and numerical errors. In addition, a comparison of corrections cannot be used to assess which method actually performs a better correction of the test data. Therefore, soon after the completion of the software and procedure development of TWICS, it became clear that a direct validation of the computed wall interference corrections, i.e. a comparison of corrected aerodynamic coefficients, was urgently needed in order to gain confidence in the magnitude of the predicted corrections.

In principle, three methods exist that may be used to perform a direct validation of a wall interference correction system for a slotted wall wind tunnel: *Method 1* $\Longrightarrow$ a test article is tested in the slotted wall wind tunnel and in a closed wall wind tunnel of similar or greater cross–sectional area; *Method 2* $\Longrightarrow$ geometrically identical test articles of different sizes are tested in the slotted wall wind tunnel; *Method 3* $\Longrightarrow$ a test article is tested in a

slotted wall wind tunnel with variable boundary conditions. In all these cases aerodynamic coefficients should theoretically agree after wall interference corrections are applied. Each of the three methods, however, has advantages and disadvantages.

Method 1 appears to be the most straight forward approach. One and the same model is tested in two tunnels that have different boundary conditions and size. The validation of TWICS will require data that is taken up to a Mach number of approximately 0.90. This Mach number, however, is outside of the range of most large closed wall wind tunnels. In addition, if a closed wall tunnel of similar size is selected, a wall interference correction system has to be in place that uses wall pressure measurements. Only in this case a comparison of corrected data sets from both tunnels is possible.

Method 2 avoids most problems associated with *Method 1.* Fabricating geometrically identical wind tunnel models of different size, however, can be very challenging and expensive. Model support system interference issues also become a major concern as a different support system adapter has to be designed for each model.

Method 3 is essentially a variation of a strategy that was used by *Iyer and Everhart*[4] to validate WICS for the closed wall test section configuration of the National Transonic Facility at Langley Research Center. They compared corrected aerodynamic coefficients recorded for the closed wall test section configuration with corresponding uncorrected coefficients recorded for the alternate slotted wall test section configuration. Their semispan model test was conducted at a very low Mach number (0.21). Consequently, they assumed that data taken during the slotted wall runs had negligible wall interference corrections. This assumption, however, cannot be used during the validation of a wall interference correction system that estimates corrections at high subsonic Mach numbers. Then, wall interference corrections caused by the interaction of the test article with the slotted wall test section are significant. They have to be applied to uncorrected tunnel conditions and aerodynamic coefficients. Therefore, a more general version of *Method 3* must be used for the validation that may be described as follows: (i) at first, the model is tested in the slotted wall test section over the selected Mach number range; (ii) in the next step, the closed wall boundary condition is imposed by covering the test section slots; (iii) then, the model is tested again over the same Mach number range; (iv) finally, wall interference corrections are computed for both test section configurations and applied to both uncorrected data sets.

Method 3 was chosen by the authors for the validation of TWICS as this method appeared to be the simplest and most accurate approach. The method offers additional advantages: (i) test data bias errors associated with the installation of the test article in two different tunnels are avoided; (ii) no change of the model support system is required; (iii) the same data system and instrumentation is used to record test data; (iv) the same wall pressure measurement system is used to estimate wall interference effects for the closed and slotted wall test section configuration.

In the spring of 2002 a detailed plan was prepared that would use data from the test of a large semispan model for a direct validation of TWICS. A simple wing–body configuration

of the model and six Mach numbers (i.e. 0.40, 0.70, 0.75, 0.80, 0.83, and 0.85) were selected for the validation test. TWICS would be used to estimate wall interference corrections for the slotted and closed wall portion of the test.

Some additional preparations were required in order to conduct the closed wall portion of the test: (i) a perturbation velocity database file satisfying the closed wall boundary condition had to be computed using panel method code ANTARES[5,6] in combination with the POLARIS[7] software package; (ii) an alternate procedure for controlling the Mach number for the closed wall portion of the test had to be developed as the plenum chamber pressure of the test section could no longer be used for this purpose; (iii) wall pressure port calibrations for the closed wall test section configuration had to be obtained.

Empty tunnel runs of both test section configurations were performed in order to determine clear tunnel static pressure gradients. These gradients were used to estimate clear tunnel buoyancy corrections. A data reduction program was written that applied all first and second order wall interference corrections to uncorrected tunnel conditions, angles, and aerodynamic coefficients. This program also contained an algorithm that performed an interpolation of the corrected aerodynamic coefficients such that the corrected Mach number for a given run would be constant.

In the next section of this report the validation test is described in greater detail. Then, the calculation of wall interference corrections is explained. This is followed by a section that discusses the least squares fit of wall signatures and shows how wall interference corrections were applied to test data. This also includes a description of the algorithm that was used to interpolate corrected aerodynamic coefficients. Finally, results of the validation test are discussed.

DESCRIPTION OF VALIDATION TEST

Test Section Geometry

Figure 1 shows the layout of the test section of the Ames 11–Foot TWT. The test section has a width and height of 11 ft (132 in). A total of 52 slots are evenly distributed over both side walls, floor, and ceiling giving the test section a porosity of 6 %. The total length of the slotted portion of the test section is 22 ft (264 in). The first 4 ft (48 in) of each slot are tapered. Fullspan models are mounted on a rear sting support system. Semispan models are installed on the floor of the test section using a turntable model support system. Slots on the floor are sealed during semispan model tests in order to provide a solid image plane. The balance center of a typical fullspan model is $\approx$ 13 ft (156 in) downstream of the start of the slotted portion of the test section. The balance center for semispan models is identical with the axis of the turntable. This axis is located $\approx$ 8.83 ft (106 in) downstream of the start of the slotted portion of the test section.

In the year 2000 a system was installed in the test section of the 11–Foot TWT that provides highly accurate wall pressure measurements to TWICS for the purpose of computing wall interference corrections. The system consists of 8 rows of wall pressure ports. Each row has 30 wall pressure ports. The streamwise spacing of the wall pressure ports is 1.0 ft (12 in) at the start and end of the test section. This spacing is reduced to 0.5 ft (6 in) in the vicinity of possible test article locations. Figures 2(a) and 2(b) show details of the wall pressure measurement system.

Operational experience showed that the control of the main wall pressure measurement error sources and automated quality checks of the wall signature are important features of the wall pressure measurement system. The system controls orifice errors caused by wall surface irregularity in the immediate area surrounding the orifice by subtracting an empty tunnel calibration signature from the wall signature that is measured during a model test. Calibration zero and sensitivity drift resulting from wall pressure transducer temperature change is controlled by using an electronic pressure scanning system that incorporates manufacturer determined transducer temperature calibrations. Finally, pressure coefficient scatter caused by low frequency flow unsteadiness in the wind tunnel is minimized by using identical length and size pressure tubing to connect wall orifices with the electronic pressure scanning instrumentation. This ensures that the dynamic response of each wall pressure transducer is nearly identical and that pressure measurements are all "in phase" relative to tunnel fluctuations.

Test Section Calibration

A test section calibration had to be performed before the semispan model was installed in the test section. The purpose of the calibration was (i) to develop an alternate method for setting the Mach number during the closed wall portion of the validation test, (ii) to calibrate wall pressure ports for the closed wall test section configuration, and (iii) to measure static pressure gradients on the test section floor. These gradients would be used to determine drag coefficient corrections that are caused by clear tunnel buoyancy effects in the test section of the 11–Foot TWT.

During the first part of the validation test all test section slots were covered with aluminum tape in order to impose the closed wall boundary condition on the test section walls. This test section configuration does not allow a pressure communication between the test section and the plenum chamber. The plenum chamber pressure, however, is normally used to set the Mach number at the model reference point. Therefore, for the closed wall test section configuration, a partial tunnel calibration became necessary in order to develop an alternative procedure to set the Mach number.

To accomplish the calibration, a static probe was installed near the semispan model reference point that would be used to measure the Mach number and the dynamic pressure. These probe measurements were related to a static pressure measurement on the ceiling of the test section that was located $\approx$ 20 ft upstream of the axis of the turntable. Table 1

lists tunnel conditions that were calibrated while the static probe was installed in the test section:

Table 1. Test section Mach number calibration (closed wall configuration).

Test Section Configuration	*Mach Number Set*
Closed Wall (probe installed)	0.30, 0.40, 0.60, 0.70, 0.75, 0.80, 0.83, 0.85, 0.90

After the completion of the Mach number calibration, tables were prepared for the facility control system so that the upstream ceiling pressure could be used to set the test section Mach number for the closed wall test section configuration.

In the next step, the static probe was removed in order to perform the second part of the test section calibration, i.e. the calibration of the wall pressure ports. This calibration is used to remove the orifice error from the wall pressure signature. Static pressures on the floor were also measured during this calibration phase so that clear tunnel buoyancy corrections for the closed wall test section configuration could be determined. Wall pressure port rows 4 and 5 were used for this purpose (see Fig. 2(b)). Table 2 shows tunnel conditions that were selected for the wall pressure port calibration of the closed wall test section configuration:

Table 2. Wall pressure port calibration (closed wall configuration).

Test Section Configuration	*Mach Number Set*
Closed Wall (probe removed)	0.30, 0.40, 0.60, 0.70, 0.75, 0.80, 0.83, 0.85, 0.90

Finally, after the aluminum tape covering the slots was removed, static pressures on the test section floor were measured for a second time. These measurements were used to develop a clear tunnel buoyancy correction procedure for the slotted wall test section configuration. Table 3 shows tunnel conditions that were used during the clear tunnel buoyancy determination for the slotted wall test section configuration:

Table 3. Clear tunnel buoyancy (slotted wall configuration).

Test Section Configuration	*Mach Number Set*
Slotted Wall (probe removed)	0.30, 0.40, 0.60, 0.70, 0.75, 0.80, 0.83, 0.85, 0.90

Clear tunnel buoyancy corrections for the closed and slotted wall portion of the TWICS validation test were determined using identical procedures. This ensured that errors associated with the application of clear tunnel buoyancy corrections to the closed and slotted wall test data would be kept to a minimum.

Wind Tunnel Model

A simple wing–body configuration of a large semispan model of The Boeing Company was used for the validation test. The model was mounted on the turntable support system. Wing flaps and slats were retracted and no engine nacelle, landing gear, or tail were attached to the semispan model. The total length of the model was $\approx$ 17 ft (204 in). The semispan of the wing was $\approx$ 8 ft (96 in). The distance between the nose of the semispan model and the beginning of the slotted portion of the test section was $\approx$ 1 ft (12 in). The distance between the wing tip and the test section ceiling was $\approx$ 3 ft (36 in). Principal dimensions and test section location of the semispan model are shown in Figure 3.

Test Matrix

The semispan model was installed in the test section after the second part of the calibration of the closed wall test section configuration was completed (see Table 2). Then, validation test data was recorded. At first, all runs of the closed wall configuration were performed. In this case, the alternate method to set the reference Mach number in the test section was used (upstream ceiling pressure). In the next step, the tape covering the slots was removed and the slotted wall runs were conducted. This time, the plenum chamber pressure was used to set the reference Mach number.

Preliminary estimates of the Mach number correction at zero lift were available for both the closed and slotted wall configuration. They were used to set the uncorrected Mach number for every validation run. This strategy ensured that the corrected Mach number of a given run would be as close as possible to the selected target Mach number. Then, errors associated with the interpolation of the corrected aerodynamic coefficients of a given run as a function of the corrected Mach number are kept to a minimum. Table 4 lists uncorrected and estimated corrected Mach numbers for the closed and slotted wall configuration:

Table 4. Uncorrected and Corrected Mach Numbers.

Configuration	*Uncorr. Mach Number*	*Corr. Mach Number*
Closed Wall	0.398	0.400
Closed Wall	0.690	0.700
Closed Wall	0.739	0.750
Closed Wall	0.787	0.800
Closed Wall	0.811	0.830
Closed Wall	0.829	0.850
Slotted Wall	0.400	0.400
Slotted Wall	0.701	0.700
Slotted Wall	0.751	0.750
Slotted Wall	0.802	0.800
Slotted Wall	0.833	0.830
Slotted Wall	0.854	0.850

In the next section of this report the calculation of wall interference corrections is explained in more detail.

CALCULATION OF WALL INTERFERENCE CORRECTIONS

Blockage Factor and Angle of Attack Correction

TWICS, the real–time wall interference correction system of the Ames 11–Foot TWT, uses a highly modified version of the wall signature method to compute wall interference corrections of a wind tunnel model. Wall interference corrections are determined by combining a singularity representation of the test article, lift force, pitching moment, and wall pressure measurements with numerical solutions of the wind tunnel and wall interference flow field.

TWICS uses line doublets to represent lifting effects of the test article. Solid volume and viscous wake blockage effects are represented by chains of point doublets. The initial location of all singularities has to be specified by using drawings of the test article. Line doublets should be located along the 1/4 chord line of the wing of the test article. Equally spaced point doublets should be placed along the test article centerline in order to model solid volume blockage effects. In addition, chains of point doublets should be placed where flow separation is expected on the test article. These point doublets model viscous wake blockage effects. Table 5 lists singularities that TWICS uses to represent a typical semispan model.

Table 5. Singularity representation of a semispan model.

Phenomenon	*Singularity Type*	*Index Range*
Lifting Effect	Line Doublet	$1 \longrightarrow \eta$
Solid Volume Blockage	Chain of Point Doublets	$\eta + 1 \longrightarrow \xi$
Viscous Wake Blockage	Chain of Point Doublets	$\xi + 1 \longrightarrow n$

TWICS derives the strength of singularities representing the semispan model from the lift force, pitching moment, and wall pressure signature measurement. The flow chart in Fig. 4 summarizes how TWICS is applied to a semispan model in the 11–Foot TWT.

TWICS needs wall signatures to determine the strength of point doublets that represent blockage effects of the test article. Therefore, a wall pressure measurement system was installed in the 11–Foot TWT that provides wall signatures to TWICS in real–time. The wall pressure measurement system consists of 240 wall pressure ports that are arranged in 8 rows with 30 ports each (see Figs. 2(a) and 2(b)). Ports belonging to rows 4 and 5 are located on the test section floor. These ports are not used by TWICS during semispan model tests as the test section floor is the image plane of the model.

After the strength of all test article singularities has been determined by TWICS, first order wall interference corrections, i.e. the blockage factor and the angle of attack correction, are computed at model reference points that are specified by the user. The blockage factor ε and the angle of attack correction α_i are linear functions of the singularity representation of the test article. The principle of superposition may be applied to the wall interference flow field. Therefore, it is possible to express ε and α_i at a model reference point ν as the sum of contributions of all singularities that represent the test article. Assuming that a total number of n singularities is used, we get for the blockage factor and the angle of attack correction:

$$\varepsilon(\nu) \quad = \quad \frac{\Delta u(\nu)}{U'} \quad = \quad \sum_{k=1}^{n} \sigma_k \cdot \overline{u_i}(\nu, k) \tag{1a}$$

$$\alpha_i(\nu) \quad = \quad \frac{\Delta v(\nu)}{U'} \quad = \quad \sum_{k=1}^{n} \sigma_k \cdot \overline{v_i}(\nu, k) \tag{1b}$$

where $\overline{u_i}(\nu, k)$ and $\overline{v_i}(\nu, k)$ are dimensionless perturbation velocities of the wall interference flow field that are caused by unit strength test article singularities. Perturbation velocity $\overline{u_i}(\nu, k)$ is the dimensionless axial perturbation velocity component at a flow field point "ν" that is caused by a singularity "k". Similarly, $\overline{v_i}(\nu, k)$ is the corresponding normalized perturbation velocity component that is perpendicular to the wing plane of the test article. The unit of $\overline{u_i}$ and $\overline{v_i}$ equals the inverse of the unit of the singularity strength.

Perturbation velocities $\overline{u_i}(\nu, k)$ and $\overline{v_i}(\nu, k)$ are computed using panel code ANTARES in combination with the POLARIS software package. In principle, this calculation is performed as follows: (i) at first, unit strength point doublets and line doublets are distributed on a cartesian grid in the test section; (ii) then, ANTARES computes the wind tunnel and wall interference flow field of each point doublet or line doublet by solving the subsonic potential equation; each flow field solution satisfies boundary conditions that describe the test section of the 11–Foot TWT; (iii) finally, the POLARIS software package is used to store these solutions in a perturbation velocity database file. TWICS ultimately scales, superimposes, and interpolates these precomputed flow field solutions in order to obtain a real–time solution of the wall interference flow field.

In general, strengths of test article singularities, i.e. σ_k in Eqs. (1a) and (1b), are calculated using the measurement of the lift force, the pitching moment, and the wall pressure signature. The calculation of the singularity strength values is essentially performed in two steps: (i) at first, the strength of each line doublet is computed by using the *Kutta/Joukowski* formula; (ii) in the next step, the strength of each point doublet is computed by applying a global least squares fit to the blockage part of the wall signature. The singularity strength calculation may be summarized as follows:

Step 1 – Line doublet strength and the Kutta/Joukowski formula: Strengths $\sigma_1, \cdots, \sigma_\eta$ of line doublets representing lifting effects of the test article are estimated by combining lift force and pitching moment measurements with the *Kutta/Joukowski* formula (for more detail see Ref. [2], App. 5). During the TWICS validation test no tail surface was attached

to the semispan model. Therefore, only the lift force measurement was needed to determine the strength of the line doublets. Weighting factors w_k were introduced that model an elliptic lift distribution along the semispan wing. Then, we get:

$$\sigma_k \;=\; w_k \cdot \frac{L' \cdot U'}{2 \cdot q'} \quad ; \quad 1 \;\leq k \;\leq\; \eta \tag{2a}$$

$$\sum_{k=1}^{\eta} w_k \quad = \quad 1 \tag{2b}$$

where L', q', and U' are the uncorrected lift force, dynamic pressure, and reference velocity.

Step 2 – Point doublet strength and the global least squares fit of the wall signature: Solid volume blockage effects of the test article are represented by a chain of equally spaced point doublets (indices $\eta+1, \cdots, \xi$). These point doublets are placed along the test article centerline, i.e. along the floor of the test section. The unknown singularity strength values $\sigma_{\eta+1}, \cdots, \sigma_\xi$ are reduced to a single variable σ_* by introducing weighting factors $w_{\eta+1}, \cdots, w_\xi$. These weighting factors are proportional to the cross–sectional area of the test article at the location of each point doublet. Then, we get the following expression:

$$\frac{\sigma_k}{\sigma_*} \quad = \quad w_k \quad \approx \quad A_k \quad ; \quad \eta + 1 \;\leq k \;\leq\; \xi \tag{3}$$

Viscous wake blockage effects are represented by another set of point doublets (indices $\xi + 1, \cdots, n$). These point doublets should be arranged in chains starting at points on the test article where flow separation is expected. Again, weighting factors are introduced to reduce the number of independent variables that are required for the calculation of the singularity strength values. Then, assuming that σ_{**} is a common reference strength, we get for the strength of each point doublet of the viscous wake:

$$\frac{\sigma_k}{\sigma_{**}} \quad = \quad w_k \quad ; \quad \xi + 1 \;\leq k \;\leq\; n \tag{4}$$

In most applications weighting factors $w_{\xi+1}, \cdots, w_n$ may be set to 1.0. The calculation of the strength of point doublets representing solid volume and viscous wake blockage effects of the semispan model is reduced to finding σ_* and σ_{**}.

A global least squares fit of the wall pressure signature is used to calculate σ_* and σ_{**}. TWICS uses the wall pressure signature expressed as a dimensionless flow velocity difference in this least squares fit. Therefore, it is necessary to compute an axial velocity U_t at each wall pressure port δ that is derived from corresponding static pressure measurements. In compressible flow, this axial velocity is given by the equation:

$$U_t(\delta) = \sqrt{\frac{2\;\gamma\;R\;T_T}{\gamma\;-\;1} \cdot \left[1 - \left(\frac{p_t(\delta)}{p_T}\right)^{\frac{\gamma-1}{\gamma}}\right]} \tag{5a}$$

where p_t is the static pressure measured at the wall pressure port δ during the wind tunnel test. The velocity U_t is corrected for orifice error, wall divergence, and wall boundary layer growth by subtracting the velocity U_c that was measured at each wall pressure port during a corresponding empty tunnel calibration. Similar to Eq. (5a), we get for the velocity U_c:

$$U_c(\delta) = \sqrt{\frac{2\ \gamma\ R\ T_T}{\gamma\ -\ 1} \cdot \left[1 - \left(\frac{p_c(\delta)}{p_T}\right)^{\frac{\gamma-1}{\gamma}}\right]} \tag{5b}$$

where p_c is the static pressure measured at the wall pressure port δ during the calibration. It is important to remember that U_c may only be subtracted from U_t if both velocities were measured at the same reference Mach number and total pressure (see Ref. [8]).

It is assumed that measurements at a total number of m wall pressure ports are used for the least squares fit of the wall pressure signature. A total number of n singularities were selected to represent the test article. Then, the normal equation of the global least squares fit may be written as[9]

$$\left[\mathbf{A^T}_{2\times m} \circ \mathbf{A}_{m\times 2}\right] \circ \mathbf{X}_{2\times 1} \ = \ \mathbf{A^T}_{2\times m} \circ \mathbf{B}_{m\times 1} \tag{6a}$$

where

$$\mathbf{X}_{2\times 1} \quad = \quad \begin{pmatrix} \sigma_* \\ \sigma_{**} \end{pmatrix} \tag{6b}$$

$$\mathbf{A}_{m\times 2} \quad = \quad \begin{pmatrix} a_{1,1} & a_{1,2} \\ \vdots & \vdots \\ a_{m,1} & a_{m,2} \end{pmatrix} \tag{6c}$$

$$a_{\delta,1} \quad = \quad \sum_{k=\eta+1}^{\xi} w_k \cdot \overline{u_t}(\delta,k) \tag{6d}$$

$$a_{\delta,2} \quad = \quad \sum_{k=\xi+1}^{n} w_k \cdot \overline{u_t}(\delta,k) \tag{6e}$$

$$\mathbf{B}_{m\times 1} \quad = \quad \begin{pmatrix} b_1 \\ \vdots \\ b_m \end{pmatrix} \tag{6f}$$

$$b_\delta \ = \ \frac{U_t(\delta)\ -\ U_c(\delta)}{U'} \ - \ \sum_{k=1}^{\eta} \sigma_k \cdot \overline{u_t}(\delta,k) \tag{6g}$$

The vector $\mathbf{X}$ contains reference strength values of singularities describing solid volume and viscous wake blockage effects. The matrix $\mathbf{A}$ contains normalized perturbation velocities of the wind tunnel flow field. The vector $\mathbf{B}$ contains the blockage part of the measured

wall signature. This part of the wall signature is obtained by subtracting line doublet contributions (indices $1, \cdots, \eta$) from the measured wall signature difference between wind tunnel flow field and empty tunnel calibration.

Perturbation velocity $\overline{u_t}(\delta, k)$ is the dimensionless perturbation velocity of the wind tunnel flow field at a wall pressure port "δ" that is caused by a unit strength singularity "k". The unit of $\overline{u_t}$ equals the inverse of the unit of the singularity strength. Similar to $\overline{u_i}(\nu, k)$ and $\overline{v_i}(\nu, k)$, panel method code ANTARES may be used to compute $\overline{u_t}(\delta, k)$ as a function of the singularity type and possible singularity locations. Perturbation velocities are again stored in a database file that is used by TWICS for interpolation purposes. Table 6 lists differences between $\overline{u_i}(\nu, k)$, $\overline{v_i}(\nu, k)$, and $\overline{u_t}(\delta, k)$.

Table 6. Perturbation Velocity Differences.

Velocity	*Flow Field Type*	*Point Type*
$\overline{u_i}(\nu, k)$, $\overline{v_i}(\nu, k)$	Wall Interference Flow Field	Reference Point
$\overline{u_t}(\delta, k)$	Wind Tunnel Flow Field	Wall Pressure Port

The solution of the least squares problem defined in Eq. (6a) may be written in explicit form as:

$$\mathbf{X}_{2\times 1} \;=\; \left[\mathbf{A}^{\mathbf{T}} \circ \mathbf{A}\right]^{-1}_{2\times 2} \;\circ\; \left[\mathbf{A}^{\mathbf{T}} \circ \mathbf{B}\right]_{2\times 1} \tag{7}$$

The solution vector $\mathbf{X}$ is computed by using a linear system solver. Then, type, location, and strength (i.e. $\sigma_1, \cdots, \sigma_n$) of all singularities representing the semispan model are known. It is now possible to determine the first order wall interference corrections, i.e. the blockage factor ε and the angle of attack correction α_i, at each reference point ν using Eqs. (1a) and (1b).

Clear Tunnel Buoyancy

Estimates of the static pressure gradient for the closed and slotted wall test section configuration of the 11–Foot TWT were obtained in order to determine clear tunnel buoyancy corrections that have to be applied to drag forces and coefficients. Static pressure measurements on the test section floor, i.e. on wall pressure port rows 4 and 5, were used to determine this pressure gradient as these two rows are located in close proximity to the centerline of the semispan model fuselage (see Fig. 2(b)).

The static pressure gradient was determined in several steps. At first, for each Mach number and test section configuration, a straight line was fitted to the pressure coefficient that was measured on rows 4 and 5. Then, the arithmetic average of the slope on rows 4 and 5 was computed for each Mach number and test section configuration. Finally, a least squares fit was applied to the pressure coefficient slope in order to obtain a closed

form solution of the slope as a function of the Mach number. The following least squares approximation of the static pressure coefficient slope was obtained for the closed wall test section configuration (see Fig. 5(a)):

$$\frac{d\ c_p}{d\ x}\ [1/ft] \quad \approx \quad 4.18 \times 10^{-4} \quad + \quad 1.15 \times 10^{-4} \ \cdot \ M \\ + \quad 1.10 \times 10^{-6} \ \cdot \ exp\ (7.5 \cdot M) \tag{8a}$$

Similarly, for the slotted wall test section configuration, the following expression for the static pressure coefficient slope was obtained (see Fig. 5(b)):

$$\frac{d\ c_p}{d\ x}\ [1/ft] \quad \approx \quad 3.85 \times 10^{-4} \quad + \quad 7.01 \times 10^{-4} \ \cdot \ M \\ - \quad 2.16 \times 10^{-3} \ \cdot \ M^2 \quad + \quad 9.47 \times 10^{-4} \ \cdot \ M^3 \tag{8b}$$

The clear tunnel buoyancy correction to the drag coefficient is simply obtained by multiplying the pressure coefficient slope by the test article volume and dividing the result by the reference area. The test article volume and the reference area of the semispan model must be compatible. In other words, the reference area of the semispan model must be half of the reference area of the corresponding fullspan model if the test article volume is half of the volume of the corresponding fullspan model.

CORRECTION OF WIND TUNNEL TEST DATA

Tunnel Conditions, Angle of Attack, and Aerodynamic Coefficients

In general, wall interference corrections are not constant along the fuselage, wing, and tail surface of a wind tunnel model. Therefore, it is required to compute weighted mean values of corrections for different sets of model reference points. Only these mean values should be used to correct tunnel conditions, the angle of attack, and aerodynamic coefficients.

First order wall interference corrections, i.e. the blockage factor and the angle of attack correction, may be computed at each model reference point after the strength of all singularities was determined. During the TWICS validation test a total of $\lambda+\mu$ model reference points were selected for the wall interference calculation. These points were located along the 1/4 and 3/4 chord line of the semispan model wing. The following index ranges were selected for the two reference point sets:

$$1 \ \leq \ \nu \ \leq \ \lambda \qquad (1/4\ chord\ line)$$
$$\lambda+1 \ \leq \ \nu \ \leq \ \lambda+\mu \qquad (3/4\ chord\ line)$$

Using past experience it was decided to compute the blockage factor ε on model reference points that were located along the 3/4 chord line. The angle of attack correction α_i, on the other hand, was computed on reference points that were located along the 1/4 and the

3/4 chord line. Weighted mean values $\overline{\varepsilon}$, $\Delta\alpha_{0.25}$, and $\Delta\alpha_{0.75}$ of the blockage factor and of the angle of attack correction were determined. These mean values are defined by the following equations:

$$\overline{\varepsilon} \quad = \quad \sum_{\nu=\lambda+1}^{\lambda+\mu} \omega_\nu \cdot \varepsilon(\nu) \tag{9a}$$

$$\Delta\alpha_{0.25} \quad = \quad \sum_{\nu=1}^{\lambda} \omega_\nu \cdot \alpha_i(\nu) \tag{9b}$$

$$\Delta\alpha_{0.75} \quad = \quad \sum_{\nu=\lambda+1}^{\lambda+\mu} \omega_\nu \cdot \alpha_i(\nu) \tag{9c}$$

where $\omega_1, \cdots, \omega_{\lambda+\mu}$ are weighting factors that are a function of the lift distribution of the semispan model wing. They fulfill the condition:

$$\sum_{\nu=1}^{\lambda} \omega_\nu \;=\; \sum_{\nu=\lambda+1}^{\lambda+\mu} \omega_\nu \;=\; 1 \tag{9d}$$

Local corrections at model reference points were used to estimate a variety of second order wall interference corrections. The calculation of a wall interference induced buoyancy correction to the drag coefficient was also included in these higher order correction estimates (for more detail see Ref. [10]). In addition, pitching moment coefficient corrections due to (i) the difference between the mean and local angle of attack correction in the spanwise direction of the wing and due to (ii) wall interference induced streamline curvature in the chordwise direction of the wing were computed (for more detail see Ref. [2], App. 18).

First and second order wall interference corrections were applied to the uncorrected test data in order to determine the corrected Mach number, dynamic pressure, and aerodynamic coefficients for a data point. Wall interference corrections were applied in the following order:

Step 1: The corrected Mach number was determined using the uncorrected Mach number and the averaged blockage factor (see Ref. [2], App. 1):

$$M \;\approx\; M' \cdot \left[\; 1 \; + \; \left(1 \; + \; \frac{\gamma - 1}{2} \cdot M'^2 \right) \cdot \left(\overline{\varepsilon} \; + \; \frac{3}{4} \cdot (\gamma - 1) \cdot M'^2 \cdot \overline{\varepsilon}^2 \right) \; \right] \tag{10}$$

Step 2: The corrected dynamic pressure was determined using the uncorrected dynamic pressure, Mach number, and the averaged blockage factor (see Ref. [2], App. 1):

$$q \;\approx\; q' \cdot \left[\; 1 \; + \; \left(2 \; - \; M'^2 \right) \cdot \overline{\varepsilon} \; + \; \left(1 - \frac{5}{2} \cdot M'^2 + \frac{2 - \gamma}{2} \cdot M'^4 \right) \cdot \overline{\varepsilon}^2 \; \right] \tag{11}$$

Step 3: The corrected angle of attack was determined by adding the averaged angle of attack correction along the 3/4 chord line to the uncorrected angle of attack:

$$\alpha \quad = \quad \alpha' \; + \; \Delta\alpha_{0.75} \tag{12}$$

Step 4: Lift and drag force corrections caused by the wall interference induced inclination of force vectors were computed by using the averaged angle of attack correction along the 1/4 chord line in combination with the following equations (see Ref. [2], App. 17):

$$\Delta L \quad = \quad - \; D' \cdot sin \; \Delta\alpha_{0.25} \; + \; L' \cdot [\; cos \; \Delta\alpha_{0.25} \; - \; 1 \;] \tag{13a}$$

$$\Delta D_1 \quad = \quad D' \cdot [\; cos \; \Delta\alpha_{0.25} \; - \; 1 \;] \; + \; L' \cdot sin \; \Delta\alpha_{0.25} \tag{13b}$$

Step 5: The drag force and drag coefficient correction due to clear tunnel buoyancy was determined using the measured static pressure coefficient slope of the test section. The following equations were used to compute these corrections:

$$\Delta D_2 \quad \approx \quad q \; \cdot \; \frac{d \; c_p}{d \; x} \cdot \; V \tag{14a}$$

$$\Delta c_{D_2} \quad \approx \quad \frac{d \; c_p}{d \; x} \cdot \frac{V}{S} \tag{14b}$$

where the pressure coefficient slope is given by Eqs. (8a) and (8b), V is the semispan model volume, q is the corrected dynamic pressure, and S is the semispan model reference area.

Step 6: The drag force and drag coefficient correction due to wall interference induced buoyancy was computed using the buoyancy correction algorithm that is described in Ref. [10]. The two corrections are given by the following equations:

$$\Delta D_3 \quad \approx \quad -2 \; \cdot \; q \; \cdot \int_V \; \frac{d \; \varepsilon}{d \; x} \; d \; V \quad \approx \quad -2 \; \cdot \; q \; \cdot \sum_V \frac{d \; \varepsilon}{d \; x} \cdot \Delta V \tag{15a}$$

$$\Delta c_{D_3} \quad \approx \quad \frac{-2}{S} \cdot \int_V \; \frac{d \; \varepsilon}{d \; x} \; d \; V \quad \approx \quad \frac{-2}{S} \cdot \sum_V \frac{d \; \varepsilon}{d \; x} \cdot \Delta V \tag{15b}$$

where S is the reference area and ΔV is a volume element of the test article. Numerical differentiation was used to approximate $d\varepsilon/dx$ locally along the fuselage centerline.

Step 7: Corrected lift and drag forces were computed by adding force corrections to uncorrected forces:

$$L \quad = \quad L' \; + \; \Delta L \tag{16a}$$

$$D \quad = \quad D' \; + \; \Delta D_1 \; + \; \Delta D_2 \; + \; \Delta D_3 \tag{16b}$$

Step 8: Corrected lift and drag coefficients were computed by dividing corrected forces by the corrected dynamic pressure and the reference area:

$$c_L = \frac{L}{q \cdot S} \tag{17a}$$

$$c_D = \frac{D}{q \cdot S} \tag{17b}$$

Step 9: Second order pitching moment coefficient corrections caused by the variation of the angle of attack correction in the spanwise and chordwise direction were computed by TWICS (see Ref. [2]. App. 18). These corrections were added to the pitching moment coefficient corrected for blockage. Then, we get for the corrected pitching moment coefficient

$$c_M = \frac{P}{q \cdot c \cdot S} = \frac{P'}{q \cdot c \cdot S} + \Delta c_{M1} + \Delta c_{M2} \tag{17c}$$

where Δc_{M1} is the pitching moment coefficient correction due to the angle of attack correction variation in the spanwise direction and Δc_{M2} is the pitching moment coefficient correction due to the angle of attack correction variation in the chordwise direction.

Constant Mach Number Interpolation

Corrected Mach number, angle of attack, and aerodynamic coefficients of each data point of a run are known after wall interference corrections are applied to the uncorrected data sets. Unfortunately, it is expected that the corrected Mach number of a given run is not constant after the Mach number correction is applied. Therefore, in order to compare corrected coefficient sets from the closed and slotted wall portion of the validation test, it is necessary to find an approximation of the corrected aerodynamic coefficients in the vicinity of each data point. This approximation will make it possible to select a constant corrected Mach number for a given run and compute corresponding corrected aerodynamic coefficients.

An approximation of a corrected aerodynamic coefficient in the neighborhood of its corrected Mach number can be found in several steps. At first, for a selected corrected angle of attack, the corresponding corrected aerodynamic coefficients and the corrected Mach number are found within each run by using linear interpolation. Introducing the abbreviation c_ξ for an aerodynamic coefficient ($\xi = L, D, M$), we get:

$$\overline{c_\xi}(\alpha, \zeta) = c_\xi(\alpha_1, \zeta) + \frac{c_\xi(\alpha_2, \zeta) - c_\xi(\alpha_1, \zeta)}{\alpha_2 - \alpha_1} \cdot [\, \alpha - \alpha_1 \,] \tag{18a}$$

$$\overline{M}(\alpha, \zeta) = M(\alpha_1, \zeta) + \frac{M(\alpha_2, \zeta) - M(\alpha_1, \zeta)}{\alpha_2 - \alpha_1} \cdot [\, \alpha - \alpha_1 \,] \tag{18b}$$

where α is the selected corrected angle of attack, M is the corrected Mach number, and ζ is the run index. The angles α_1 and α_2 are assumed to be the two nearest neighbors of the corrected angle of attack α.

In the next step, using the interpolated aerodynamic coefficients $\overline{c_\xi}$ and Mach numbers $\overline{M}$, the three run indices $\zeta_1, \zeta_2, \zeta_3$ are identified that are closest to the selected target Mach number of a run. Then, a parabola is fitted through these three nearest neighbors. The parabola has the following form:

$$\widehat{c_\xi}(\alpha, M) \quad = \quad a \cdot M^2 \; + \; b \cdot M \; + \; c \tag{19a}$$

where coefficients of the parabola are given as:

$$a \quad = \quad \frac{1}{\overline{M}(\alpha,\zeta_3) - \overline{M}(\alpha,\zeta_2)} \; \cdot \; \left[\frac{\overline{c_\xi}(\alpha,\zeta_3) - \overline{c_\xi}(\alpha,\zeta_1)}{\overline{M}(\alpha,\zeta_3) - \overline{M}(\alpha,\zeta_1)} \; - \; \frac{\overline{c_\xi}(\alpha,\zeta_2) - \overline{c_\xi}(\alpha,\zeta_1)}{\overline{M}(\alpha,\zeta_2) - \overline{M}(\alpha,\zeta_1)} \right] \tag{19b}$$

$$b \quad = \quad \frac{\overline{c_\xi}(\alpha,\zeta_2) \; - \; \overline{c_\xi}(\alpha,\zeta_1)}{\overline{M}(\alpha,\zeta_2) \; - \; \overline{M}(\alpha,\zeta_1)} \quad - \quad a \; \cdot \; \left[\; \overline{M}(\alpha,\zeta_1) \; + \; \overline{M}(\alpha,\zeta_2) \; \right] \tag{19c}$$

$$c \quad = \quad - \, a \; \cdot \; \overline{M}(\alpha,\zeta_1)^2 \; - \; b \; \cdot \; \overline{M}(\alpha,\zeta_1) \; + \; \overline{c_\xi}(\alpha,\zeta_1) \tag{19d}$$

The proposed Mach number interpolation algorithm can, of course, only be applied if at least three runs are processed by TWICS. These three runs should also have been recorded at Mach numbers that are at least 0.01 apart.

DISCUSSION OF RESULTS

Comparison of Wall Interference Corrections

At first, after all validation test data points were processed by TWICS, wall interference corrections for the given uncorrected Mach numbers were analyzed and compared. The following first order wall interference corrections where investigated: blockage factor, Mach number correction, and angle of attack correction on the 1/4 and 3/4 chord line. Second order wall interference corrections were also computed and applied. This included (i) pitching moment corrections caused by the difference between the mean and local angle of attack correction in the spanwise direction of the wing, (ii) pitching moment corrections caused by wall interference induced streamline curvature in the chordwise direction, and (iii) wall interference induced buoyancy corrections to the drag coefficient.

Figure 6(a) shows the blockage factor as a function of the uncorrected angle of attack and Mach number for the closed wall test data. Figures 6(b) depicts corresponding results for the slotted wall test data. In general, the magnitude of blockage corrections increases as

the angle of attack and the Mach number increase. Closed wall corrections are positive. Slotted wall corrections, on the other hand, are negative. As expected, the absolute value of the closed wall corrections is much larger than the absolute value of corresponding corrections for the slotted wall case.

Figures 7(a) shows the Mach number correction as a function of the uncorrected angle of attack and Mach number for the closed wall test data. Figures 7(b) depicts corresponding results for the slotted wall test data. As expected, Mach number correction and blockage factor show a very similar behavior. It can also be seen that Mach number corrections for a given run, i.e. for a given uncorrected Mach number, are not constant. They change as a function of the angle of attack. Therefore, in order to compare corrected aerodynamic coefficients from the closed and slotted wall portion of the validation test, it is required to interpolate corrected coefficients such that the corrected Mach number of a run is constant.

Figures 8(a) shows the angle of attack correction of the test article as a function of the uncorrected angle of attack and Mach number for the closed wall test section configuration. Figures 8(b) depicts corresponding results for the slotted wall configuration. Angle of attack corrections are positive for the closed wall test section configuration and negative for the slotted wall test section configuration. The magnitude of the angle of attack correction increases with increasing angle of attack and Mach number.

Figures 9(a) and 9(b) show pitching moment coefficient corrections for the uncorrected Mach number 0.40 and 0.83 that were computed for the closed wall test section configuration. Figures 9(c) and 9(d) show corresponding results for the slotted wall test section configuration. In case of the closed wall test section configuration, both pitching moment correction increments, i.e. Δc_{M1} and Δc_{M2}, are approximately equal in size. In case of the slotted wall test section configuration, however, the pitching moment increment Δc_{M1} caused by the difference between the mean and local angle of attack correction in the spanwise direction of the wing is responsible for 80% to 90% of the total pitching moment coefficient correction.

Figures 10(a) and 10(b) show the drag coefficient correction caused by wall interference induced buoyancy for the closed wall configuration. Corrections for an uncorrected Mach number of 0.40 and 0.83 are depicted. For a Mach number of 0.40, the drag coefficient correction varies from ± 1 to -5 drag counts. For a Mach number of 0.83, the magnitude of the drag coefficient correction is much larger and varies from -10 to -60 drag counts. It appears that the drag coefficient correction decreases with increasing angle of attack.

Figures 10(c) and 10(d) depict the drag coefficient correction caused by wall interference induced buoyancy for the slotted wall configuration. Again, corrections for an uncorrected Mach number of 0.40 and 0.83 are shown. For a Mach number of 0.40, the drag coefficient correction varies from ± 1 to -9 drag counts. For a Mach number of 0.83, the magnitude of the drag coefficient correction is much larger and varies from -10 to -20 drag counts. Overall it appears that the drag coefficient correction increases with increasing angle of attack.

Least Squares Fit of Wall Signature

An investigation of the least squares fit of the wall signature may be used to qualitatively assess the accuracy of wall interference corrections that are computed by TWICS for the closed and slotted wall test section configuration of the 11–Foot TWT. After a closer examination of Eq. ($6g$) we see that the least squares fit is only applied to the blockage part of the measured wall signature. The blockage part is simply obtained by subtracting the predicted lifting effect of the test article from the measured wall signature. Therefore, Eq. ($6g$) may also be written as

$$b_\delta \quad = \quad b_{\delta,M} \quad - \quad b_{\delta,L} \tag{20a}$$

Comparing Eq. ($20a$) with Eq. ($6g$) we see that the measured wall signature is given by the following dimensionless velocity difference:

$$b_{\delta,M} \quad = \quad \frac{U_t(\delta) \; - \; U_c(\delta)}{U'} \tag{20b}$$

Similarly, the predicted lifting effect of the test article at a wall pressure port is given by the following summation:

$$b_{\delta,L} \quad = \quad \sum_{k=1}^{\eta} \sigma_k \cdot \overline{u_t}(\delta, k) \tag{20c}$$

Strengths of all singularities representing blockage and lifting effects of the test article, i.e. $\sigma_1, \cdots, \sigma_n$, are known after the least squares problem is solved (cf. Eq. (7)). The fitted wall signature may now be computed by simply superimposing the influence of all test article singularities at each wall pressure port. Then, the fitted wall signature is given by the equation:

$$b_{\delta,F} \quad = \quad \sum_{k=1}^{n} \sigma_k \cdot \overline{u_t}(\delta, k) \tag{20d}$$

A comparison of the measured and fitted wall signature may be used to assess the accuracy of the computed wall interference corrections. The measured and fitted wall signature should satisfy the following relationship:

$$b_{\delta,M} \quad \approx \quad b_{\delta,F} \tag{20e}$$

A reasonable agreement between measured and fitted wall signature essentially means that wall interference corrections are computed using a good theoretical description of the wind tunnel flow field.

Four data points were selected from the validation test data in order to perform a comparison of the measured and fitted wall signature for typical Mach number / angle of attack combinations. Table 7 lists test section configuration, uncorrected, and corrected Mach number and angle of attack for each data point. Data points were selected such that the corrected angle of attack would be in the vicinity of 7.7°. In addition, it was made sure that pairs of closed and slotted wall configuration data points would have almost identical corrected Mach numbers.

Table 7. Description of Validation Test Data Points.

Data Point No.	*Configuration*	M'	α'	M	α
1	Closed Wall	0.40	7.0°	0.40	7.7°
2	Slotted Wall	0.40	8.0°	0.40	7.7°
3	Closed Wall	0.79	7.0°	0.83	7.7°
4	Slotted Wall	0.83	8.0°	0.82	7.6°

For the current study wall signatures were plotted on wall pressure port row 3 (below the wing plane) and row 6 (above the wing plane). Figure 2(b) depicts the circumferential location of these wall pressure port rows.

Figures 11(a) and 11(b) show the measured and fitted wall signature on row 3 and row 6 for a corrected Mach number of 0.40 in the closed wall test section. In this case, measured and fitted wall signature show excellent agreement.

Figures 11(c) and 11(d) depict the measured and fitted wall signature on row 3 and row 6 for a corrected Mach number of 0.40 in the slotted wall test section. The agreement between measured and fitted wall signature is still good. Larger difference between measured and fitted signature, however, are noticable on row 6. These differences may be caused by (i) local effects of the test article geometry on wall pressure measurements and (ii) errors caused by the theoretical description of the boundary condition of the slotted wall test section configuration.

Figures 11(e) and 11(f) show the measured and fitted wall signature on row 3 and row 6 for a corrected Mach number of 0.83 in the closed wall test section. The agreement between measured and fitted wall signature is good. Local differences between measured and fitted signature are probably caused by the formation of supersonic flow regions on the test article.

Figures 11(g) and 11(h) show the measured and fitted wall signature on row 3 and row 6 for a corrected Mach number of 0.82 in the slotted wall test section. Again, the agreement between measured and fitted wall signature is good. Larger differences between measured and fitted signature, however, are noticable on both rows. These differences are probably caused by (i) local effects of the test article geometry on these wall pressure measurements, (ii) the development of supersonic flow regions on the test article, and (iii) small errors in the theoretical description of the wall boundary conditions.

Overall, the agreement between measured and fitted wall signatures for all four data points is very good considering the fact that the least squares fit does not fit the wall signature row by row. Instead, only 2 unknowns are used in a single step to fit the entire wall signature that consists of 180 measurements.

In the next section of this report, corrected tunnel conditions and aerodynamic coefficients are compared and discussed in order to perform the direct validation of TWICS.

Comparison of Corrected Wind Tunnel Test Data

Uncorrected tunnel conditions, angle of attack, lift, drag, and pitching moment coefficients were corrected for wall interference in order to compare corrected wind tunnel test data sets and to perform a direct validation of TWICS. In addition, at high subsonic Mach numbers, corrected aerodynamic coefficients were interpolated as described above in order to make sure that all corrected coefficients of a given run have the same corrected Mach number. Corrected coefficients for the following corrected Mach numbers were analyzed: 0.40, 0.70, 0.75, 0.80, 0.83, and 0.85. Corrected aerodynamic coefficients for all these Mach numbers showed very similar characteristics. Therefore, it was decided to discuss only runs in this report that were recorded at a Mach number of 0.40 and 0.83.

For a Mach number of 0.40 only corrected aerodynamic coefficients are discussed as no interpolation of the aerodynamic coefficients was possible. In case of Mach number 0.83, however, an interpolation of the corrected coefficients was performed as corrected aerodynamic coefficients for Mach number 0.80, 0.83, and 0.85 were available for the interpolation.

Figure 12(a) shows uncorrected and corrected Mach numbers for the target Mach number 0.40 as a function of the angle of attack. Overall, it can be seen that the corrected Mach number shows only a maximum variation of $+0.002$ for the closed wall test data. Similarly, a Mach number variation of only -0.003 is observed for the slotted wall test section configuration. Therefore, for the target Mach number 0.40, changes of the aerodynamic coefficients may be neglected that are caused by wall interference induced variations of the corrected Mach number.

Figure 12(b) shows uncorrected and corrected Mach numbers as a function of the angle of attack for the target Mach number 0.83. Corrected Mach numbers show a maximum variation of $+0.025$ for the closed wall test section configuration. Similarly, a Mach number variation of -0.010 can be observed for the slotted wall test section configuration. These Mach number changes cannot be neglected. Therefore, an interpolation of the aerodynamic coefficients is required. This test data interpolation ensures that corrected aerodynamic coefficients of a given run have the same corrected Mach number.

Differences between sets of uncorrected and corrected aerodynamic coefficients were plotted during the test data analysis in order to compare results of the closed and slotted wall portion of the validation test. This approach has several advantages: (i) differences between

closed and slotted wall data make it possible to compare aerodynamic coefficients before and after wall interference corrections are applied by simply looking at two instead of four curves; (ii) differences between uncorrected and corrected coefficients are identical with the total correction that was applied to the uncorrected coefficients; (iii) improvements of the test data can be studied in detail without plotting the aerodynamic coefficients themselves.

In general, differences between uncorrected aerodynamic coefficients may easily be computed by using a piecewise linear fit. These differences may be defined as follows:

$$\delta c'_L = c'_{L,\ closed\ wall} - c'_{L,\ slotted\ wall} \tag{21a}$$

$$\delta c'_D = c'_{D,\ closed\ wall} - c'_{D,\ slotted\ wall} \tag{21b}$$

$$\delta c'_M = c'_{M,\ closed\ wall} - c'_{M,\ slotted\ wall} \tag{21c}$$

Similarly, differences between corrected aerodynamic coefficients may be defined as:

$$\delta c_L = c_{L,\ closed\ wall} - c_{L,\ slotted\ wall} \tag{22a}$$

$$\delta c_D = c_{D,\ closed\ wall} - c_{D,\ slotted\ wall} \tag{22b}$$

$$\delta c_M = c_{M,\ closed\ wall} - c_{M,\ slotted\ wall} \tag{22c}$$

Finally, differences between interpolated aerodynamic coefficients (constant corrected Mach number of a run) may be defined as:

$$\delta \widehat{c_\xi} = \widehat{c_\xi}_{,\ closed\ wall} - \widehat{c_\xi}_{,\ slotted\ wall} \quad ; \quad \xi = L, D, M \tag{23}$$

Uncorrected aerodynamic coefficients are defined as follows:

$$c'_L = \frac{L'}{q' \cdot S} \tag{24a}$$

$$c'_D = \frac{D'}{q' \cdot S} \tag{24b}$$

$$c'_M = \frac{P'}{q' \cdot c \cdot S} \tag{24c}$$

Similarly, corrected aerodynamic coefficients are defined in Eqs. (17a), (17b), and (17c). In an ideal situation, assuming that the wind tunnel model experienced the same flow field during the closed and slotted wall portion of the validation test, differences of corrected aerodynamic coefficients, i.e. δc_L, δc_D, δc_M, should be very close to zero.

Uncorrected and corrected lift coefficient differences for the selected target Mach numbers are depicted in Figs. 13(a) and 13(b). For the Mach number 0.40 no interpolation of the lift coefficient was performed as the wall interference induced Mach number variation

during the run was small (cf. Fig. 12(a)). Therefore, only uncorrected and corrected lift coefficient differences are plotted in Fig. 13(a). Differences of the corrected lift coefficients are close to zero as the corrected lift coefficients of the closed and slotted wall data sets showed excellent agreement after wall interference corrections were applied. The maximum observed variation of the corrected lift coefficient differences is on the order of 0.015.

For the target Mach number 0.83 an interpolation of the lift coefficient was performed as the wall interference induced Mach number variation during the run was very large for both the closed and slotted wall test data (cf. Fig. 12(b)). Uncorrected, corrected, and interpolated lift coefficient differences are plotted in Fig. 13(b). Comparing lift coefficient differences depicted in Fig. 13(b) it can clearly be seen that the difference of the interpolated lift coefficients is closest to zero. In other words, interpolated lift coefficients of the closed and slotted wall data sets showed the best agreement after wall interference corrections were applied. The remaining maximum variation of the interpolated lift coefficient differences is on the order of 0.020.

Uncorrected and corrected drag coefficient differences are depicted in Figs. 14(a) and 14(b). Again, for the target Mach number 0.40, no interpolation of the drag coefficient was performed. Consequently, only uncorrected and corrected drag coefficient differences are plotted in Fig. 14(a). For the Mach number 0.40 differences of the corrected drag coefficients are on the order of 1 to 3 drag counts up to an angle of attack of $\approx 7^\circ$. In this angle of attack range, corrected lift coefficients of the closed and slotted wall data sets showed excellent agreement after wall interference corrections were applied. For angles of attack between 7° and 12° differences of the corrected drag coefficients steadily increase up to 70 drag counts.

An interpolation of the drag coefficient at Mach number 0.83 was performed. Uncorrected, corrected, and interpolated drag coefficient differences for this Mach number are plotted in Fig. 14(b). Again, comparing drag coefficient differences depicted in Fig. 14(b), we see that the difference of the interpolated drag coefficients is closest to zero. Interpolated drag coefficients of the closed and slotted wall data sets showed the best agreement after wall interference corrections were applied. Differences of 5 to 30 drag counts remain after the interpolation of the corrected drag coefficients.

During the analysis of the test data a study was performed to validate the magnitude of the estimated buoyancy correction. Therefore, drag coefficients were investigated in more detail that were measured in the vicinity of zero lift. In this case, only three corrections have to be applied to the uncorrected drag coefficient: (i) the dynamic pressure correction, (ii) the clear tunnel buoyancy correction, and (iii) the wall interference induced buoyancy correction. During the study, four different cases for each of the two target Mach numbers were investigated. At first, only the dynamic pressure correction was applied to the drag coefficient (*Case 1*). In the next step, dynamic pressure and clear tunnel buoyancy correction were applied (*Case 2*). Then, dynamic pressure and wall interference induced buoyancy correction were applied (*Case 3*). Finally, all corrections, i.e. dynamic pressure, clear tunnel buoyancy, and wall interference induced buoyancy correction, were applied to uncorrected drag coefficients (*Case 4*).

Corrected drag coefficient differences are depicted in Fig. 15(a) for the target Mach number 0.40. Coefficients were again interpolated for target Mach number 0.83 as wall interference induced changes of the corrected Mach number could not be neglected. Corresponding interpolated drag coefficient differences are depicted in Fig. 15(b). Comparing the corrected/interpolated drag coefficient differences shown in Figs. 15(a) and 15(b) we see that differences computed for *Case 4* are closest to zero for the data point that corresponds to zero lift ($\approx -2^\circ$ angle of attack for target Mach number 0.40 and $\approx -1.5^\circ$ angle of attack for target Mach number 0.83). Thus, corrected/interpolated drag coefficients show the best agreement only after dynamic pressure, clear tunnel, and wall interference induced buoyancy correction are applied.

From Figs. 10(a) to 10(d) we know that the drag coefficient correction for wall interference induced buoyancy was -1 and -11 drag counts for the closed wall data and -8 and -18 drag counts for the slotted wall data. The application of the wall interference induced buoyancy correction to the drag coefficient made sure that the difference of the corrected drag coefficients was reduced to less than 1 drag count.

Finally, uncorrected and corrected pitching moment coefficient differences for the selected target Mach numbers are depicted in Figs. 16(a) and 16(b). Again, in the case of Mach number 0.40, no interpolation of the pitching moment coefficient was performed. Therefore, only uncorrected and corrected pitching moment coefficient differences are plotted in Fig. 16(a). Overall, the difference of the corrected pitching moment coefficients is significantly closer to zero than the difference of the uncorrected pitching moment coefficients. The application of wall interference corrections has noticably improved the agreement between pitching moment coefficients that were obtained during the closed and slotted wall portion of the validation test.

For the target Mach number 0.83 a similar result was obtained after an interpolation of the corrected pitching moment coefficients had been performed. Uncorrected, corrected, and interpolated pitching moment coefficient differences are plotted in Fig. 16(b). Comparing pitching moment coefficient differences shown in Fig. 16(b) it can be seen that the difference of interpolated coefficients is closest to zero. The interpolated pitching moment coefficients of the closed and slotted wall data sets showed the best agreement after wall interference corrections were applied.

In general, it is useful to compare the total correction that was applied to the uncorrected aerodynamic coefficient for a given angle of attack. The total correction may be computed by applying a piecewise linear fit to the uncorrected, corrected, or interpolated aerodynamic coefficients plotted as a function of the corresponding angle of attack. Then, the total correction for each coefficient may simply be computed by using the following equations:

$$\Delta c_L = c_L - c'_L \tag{25a}$$

$$\Delta c_D = c_D - c'_D \tag{25b}$$

$$\Delta c_M = c_M - c'_M \tag{25c}$$

Figures 17(a) to 19(b) show total corrections that were computed for target Mach numbers 0.40 and 0.83. Overall, comparing total corrections for the closed and slotted wall test data, we see that the magnitude of the closed wall corrections is larger than the magnitude of the slotted wall corrections. Corrections computed for the slotted wall data, however, are not small. For the slotted wall data, the following range of the lift, drag, and pitching moment coefficient correction for the target Mach number 0.83 was computed:

$$-0.0100 \leq \Delta c_L \leq +0.0500 \tag{26a}$$

$$-0.0020 \leq \Delta c_D \leq +0.0050 \tag{26b}$$

$$-0.0100 \leq \Delta c_M \leq +0.0100 \tag{26c}$$

Permissible measuring errors for aerodynamic coefficients are given in Table 8.

Table 8. Permissible measuring errors.[11]

Coefficient	*Low Angle of Attack*	*High Angle of Attack*
c_L	± 0.0010	± 0.0020
c_D	± 0.0001	± 0.0020
c_M	± 0.0010	± 0.0020

Comparing error bounds listed in Table 8 with the range of the lift, drag, and pitching moment coefficient correction given in Eqs. (26a), (26b), and (26c), we see that the magnitude of the slotted wall corrections cannot be neglected.

CONCLUSIONS

For the first time a direct validation of the wall interference correction system of the Ames 11–Foot TWT was performed. Different sets of uncorrected aerodynamic coefficients were obtained by changing the boundary condition on the test section walls. This approach appears to be a very inexpensive and accurate way of studying the absolute accuracy of wall interference correction estimates for a transonic wind tunnel as no model changes are required and simple aluminum tape may be used to cover test section slots.

Overall, the validation of TWICS was successful. Corrected lift, drag, and pitching moment coefficients for the closed and slotted wall configuration show very good agreement for the selected Mach number and angle of attack range. The magnitude of the clear tunnel and wall interference induced buoyancy correction was also validated by comparing corrected drag coefficients at zero lift before and after buoyancy corrections were applied.

Residual differences of the corrected lift, drag, and pitching moment coefficients at higher Mach numbers and angles of attack may have been caused by several sources: (1) The test

section calibration and Mach number control procedure used for the closed wall portion of the validation test was not as good as procedures used for the slotted wall test section configuration. (2) The semispan model was perhaps too big for the validation test as the distance between the wing tip and test section ceiling was less than 3 ft. In addition, the nose of the fuselage was less than 1 ft downstream of the beginning of the slotted portion of the test section. (3) The location and shape of the wing wake could have been influenced by the fundamentally different character of the closed and slotted wall boundary condition. In this case, "uncorrectable" differences between corrected aerodynamic coefficients would be expected as aerodynamic coefficients of a classical wing–body configuration are very sensitive to changes in the location and shape of the wing wake. (4) More densely spaced uncorrected Mach numbers should have been used in order to reduce the numerical error associated with the interpolation of the corrected aerodynamic coefficients of a given run.

All these error sources may have contributed to the remaining differences between the corrected / interpolated coefficients. Therefore, the following recommendations for future validation tests can be made: (i) Mach number control and flow field calibrations for the closed and slotted wall portion of the validation test should be of similar quality. (ii) The span of a semispan model used for a validation test should be limited to 60 % of the width/height of the wind tunnel. (iii) A denser Mach number spacing, e.g. 0.70, 0.71, ..., 0.88, should be used during the validation test in order to reduce errors associated with the interpolation of corrected aerodynamic coefficients of a given run. (iv) A total of 30–40 data points should be taken during each run in order to improve the resolution of the lift, drag, and pitching moment coefficient curves over the whole angle of attack range.

Results of the validation test have shown the benefit of taking data at a constant corrected Mach number in order to avoid an interpolation of aerodynamic coefficients after the completion of a test. The greater the subsonic Mach number is the more critical it becomes to take test data at constant corrected Mach number. This type of test procedure, however, is only available if a transonic wind tunnel has a wall interference correction system like TWICS in place that is capable of sending an estimated corrected Mach number to the tunnel control system in real–time.

In the future it is planned to repeat the validation test using a slightly smaller semispan model and more densly spaced uncorrected Mach numbers. A test using a sting mounted fullspan model will also have to be performed in order to gain confidence in the validation approach. Before any future validation tests, however, a more accurate procedure will have to be developed to control the Mach number for the closed wall test section configuration of the 11–Foot TWT. In addition, simple procedures should be developed in order to switch the Mach number control from the plenum pressure based method for the slotted wall test section configuration to the alternate method for the closed wall configuration. A connection between TWICS and the facility control system should also be established which would make it possible to take data at constant corrected Mach number. Then, no further interpolation of the corrected aerodynamic coefficients would be required after the application of wall interference corrections to the test data. In the long run these improvements will lead to more accurate corrected tunnel conditions and aerodynamic coefficients in a transonic wind tunnel.

REFERENCES

[1] Ulbrich, N. and Boone, A. R., "Determination of the Boundary Condition of the NASA Ames 11Ft Transonic Wind Tunnel," AIAA 2001–1112, paper presented at the 39th Aerospace Sciences Meeting, Reno, Nevada, January 8–11, 2001.

[2] Ulbrich, N., "The Real–Time Wall Interference Correction System of the NASA Ames 12–Foot Pressure Wind Tunnel," NASA/CR–1998–208537, NASA Ames Research Center, Moffett Field, California, July 1998.

[3] Ulbrich, N. and Boone, A. R., "Real–Time Wall Interference Correction System of the 12Ft Pressure Wind Tunnel," AIAA 98–0707, paper presented at the 36th Aerospace Sciences Meeting, Reno, Nevada, January 12–15, 1998.

[4] Iyer, V. and Everhart, J. L., "Application of Pressure–Based Wall Correction Methods to Two NASA Langley Wind Tunnels," AIAA 2001–2472, paper presented at the 19th AIAA Applied Aerodynamics Conference, Anaheim, California, June 11–14, 2001.

[5] Ulbrich, N., "Description of Panel Method Code ANTARES," NASA/CR-2000-209592, NASA Ames Research Center, Moffett Field, California, May 2000.

[6] Ulbrich, N., "The Application of Panel Method Code ANTARES to Wind Tunnel Wall Interference Problems," AIAA 2002–0307, paper presented at the 40th AIAA Aerospace Sciences Meeting, Reno, Nevada, 14–17 January 2002.

[7] Ulbrich, N., "Description of the POLARIS Software Package," internal report, Wind Tunnel Operations Division, NASA Ames Research Center, Moffett Field, California, June 2001.

[8] Boone, A. R. and Ulbrich, N., "The Development of a Wall Pressure Measurement System for Two NASA Ames Wind Tunnels," AIAA 2002–3250, paper presented at the 22nd AIAA Aerodynamic Measurement Technology and Ground Testing Conference, St. Louis, Missouri, June 24–27, 2002.

[9] Strang, G., "Introduction to Applied Mathematics," Wellesley – Cambridge Press, Wellesley, Massachusetts, 1986, p.35–39 .

[10] Ulbrich, N., "The Buoyancy Correction Algorithm of the NASA Ames 12Ft Pressure Wind Tunnel," internal report, Aeronautical Test and Simulation Division, NASA Ames Research Center, Moffett Field, California, March 1999.

[11] Pope, A. and Rae, W. H., "Low–Speed Wind Tunnel Testing," John Wiley & Sons, Inc., 1984, p.165, Table 4.3 .

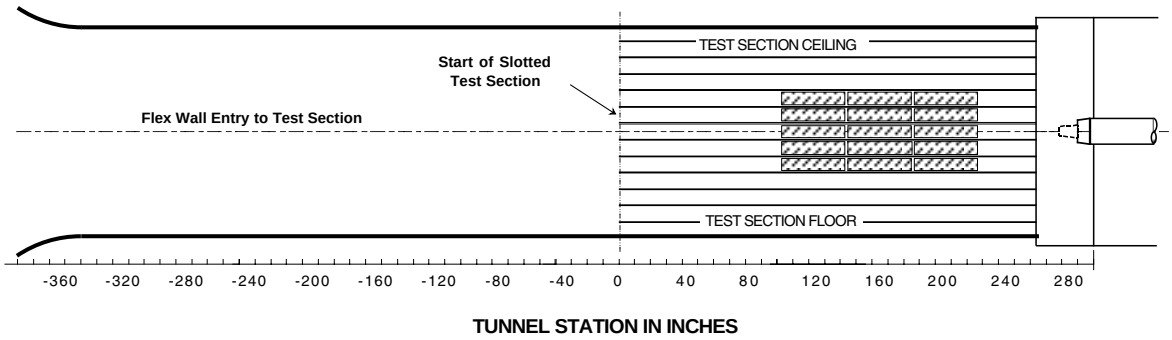

Figure 1. Test section of the Ames 11–Foot Transonic Wind Tunnel.

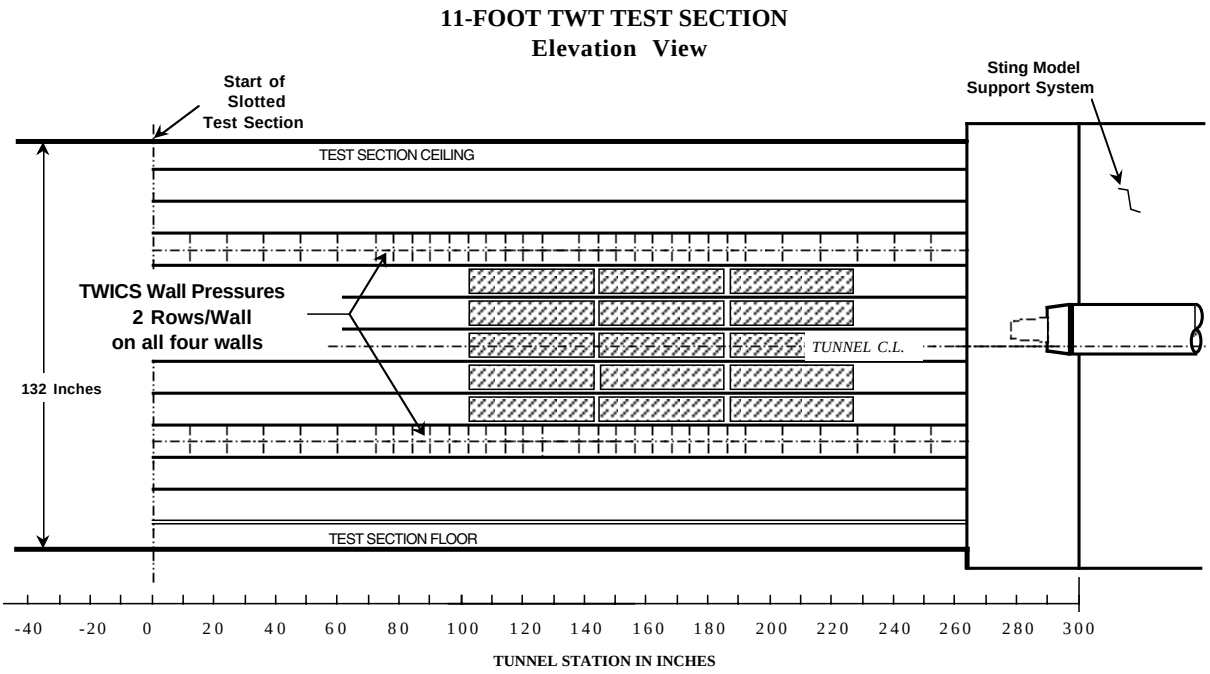

Figure 2(a). Streamwise location of wall pressure ports.

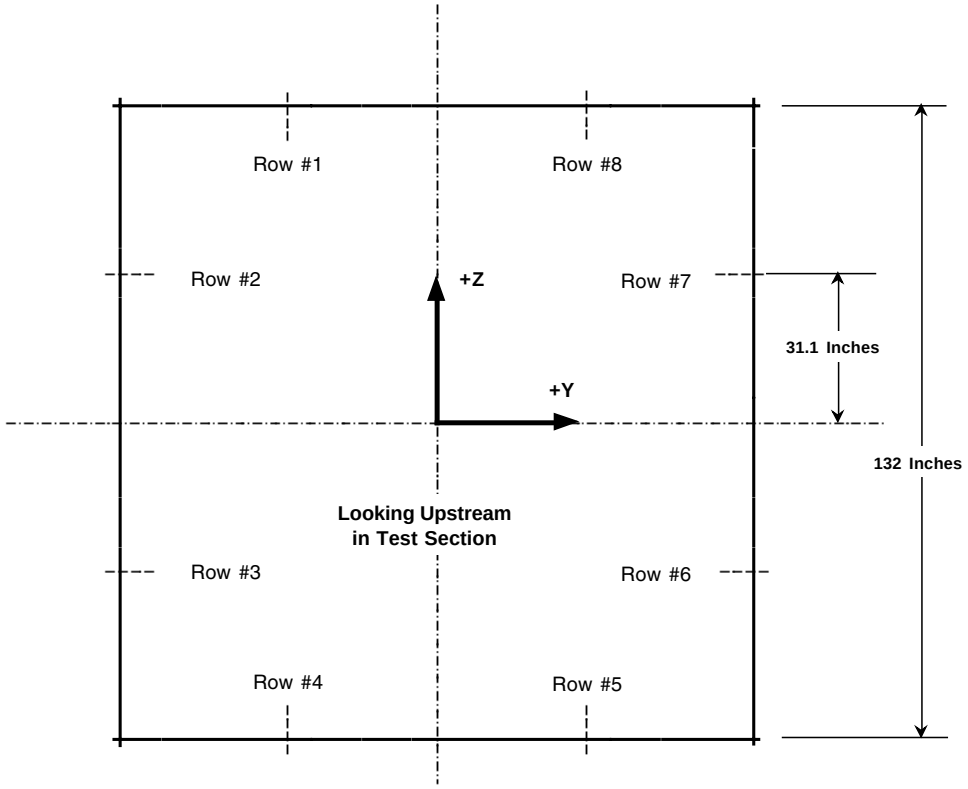

Figure 2(b). Circumferential location of wall pressure port rows.

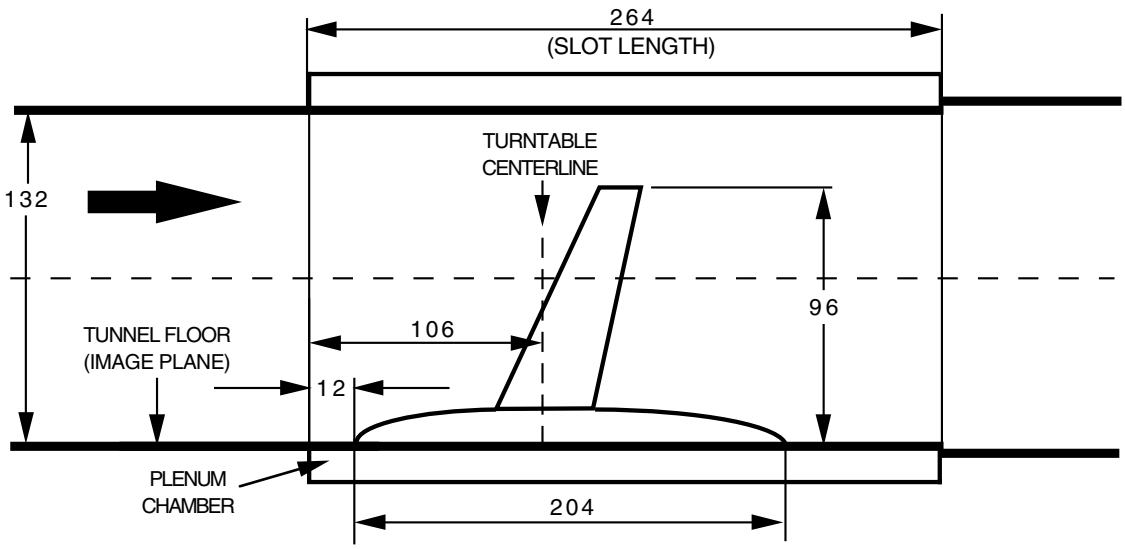

Figure 3. Location of semispan model in test section.

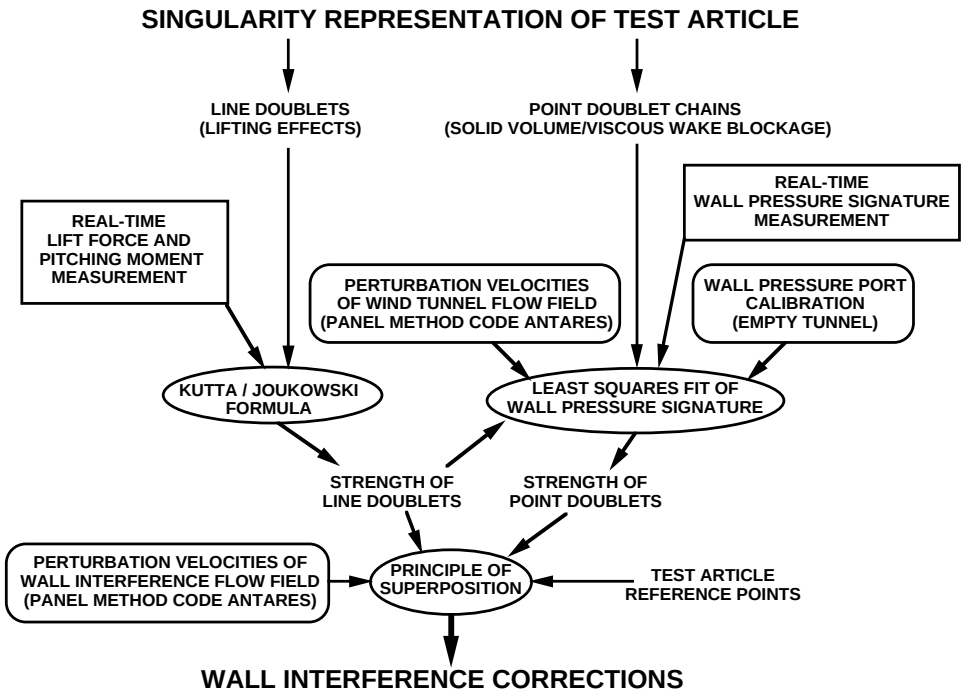

Figure 4. Real-time wall interference calculation for semispan model.

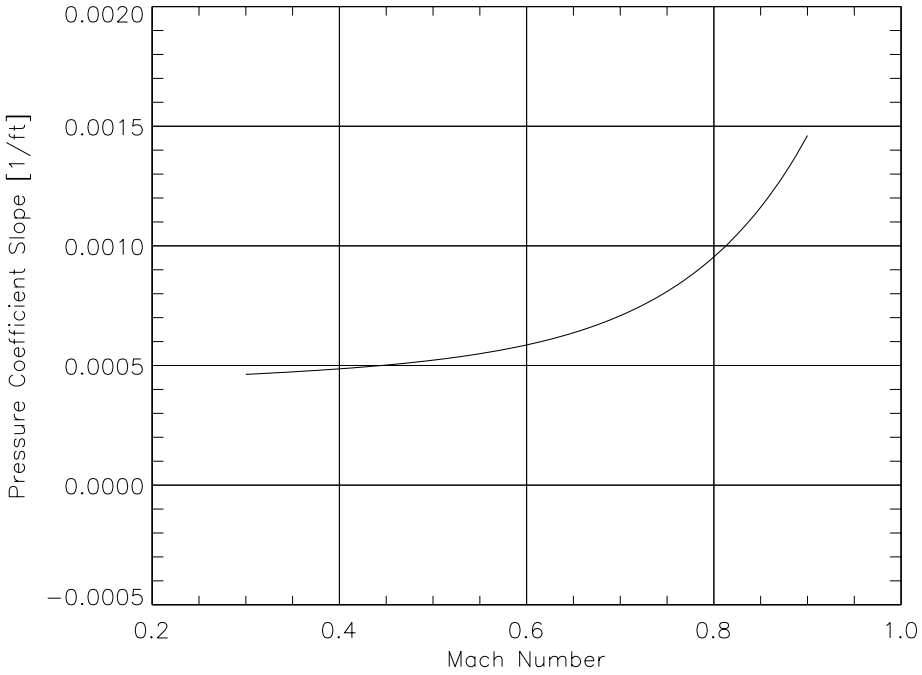

Figure 5(a). Pressure coefficient slope versus Mach number (closed wall calibration).

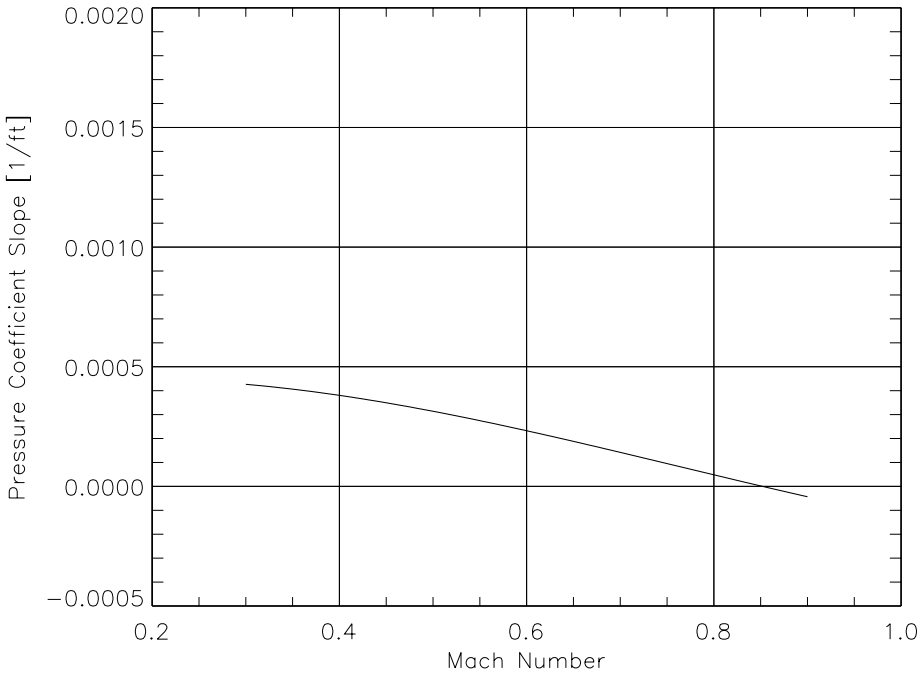

Figure 5(b). Pressure coefficient slope versus Mach number (slotted wall calibration).

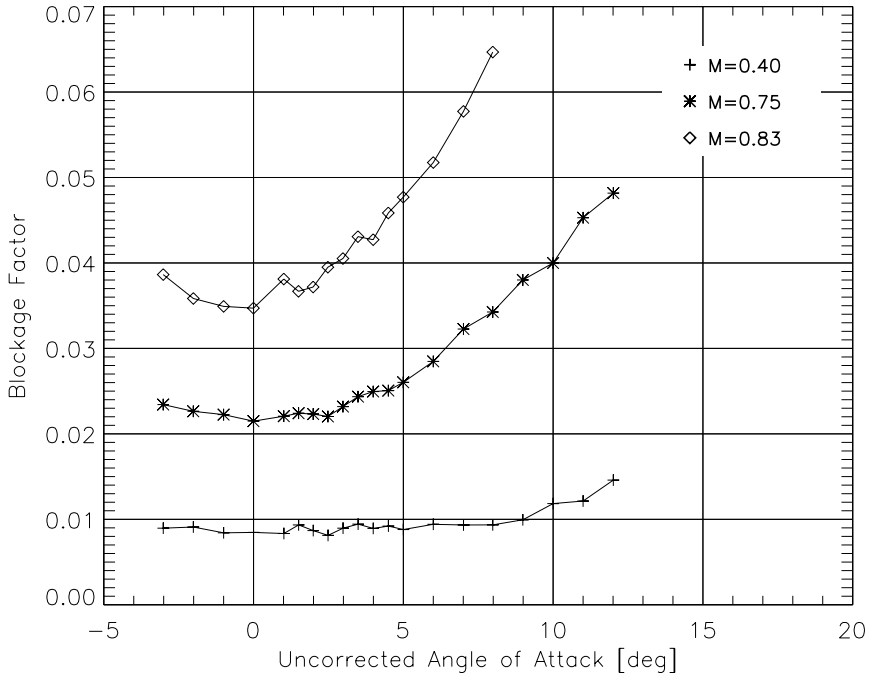

Figure 6(a). Blockage factor for closed wall configuration.

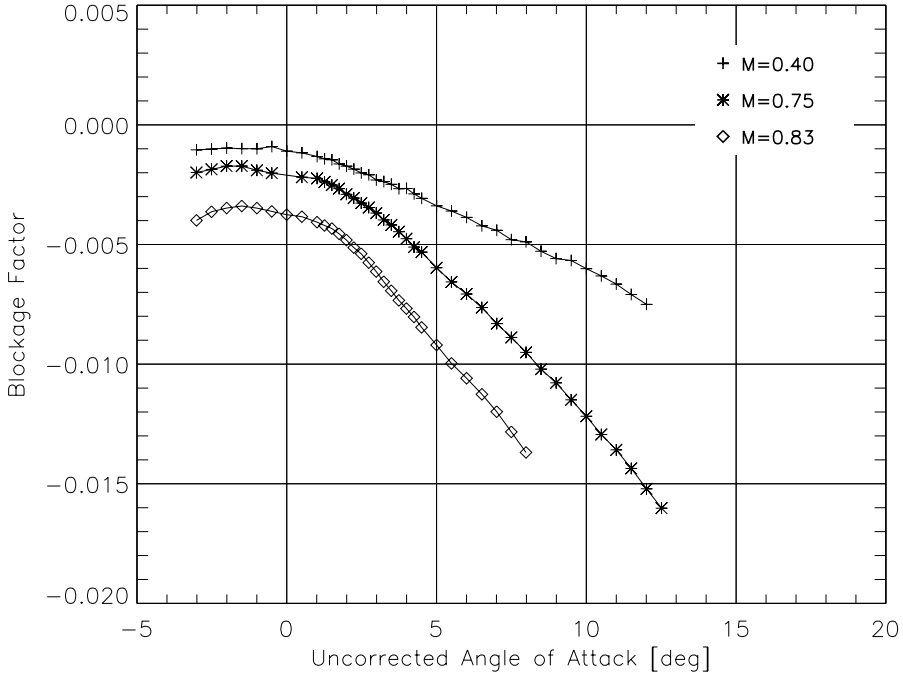

Figure 6(b). Blockage factor for slotted wall configuration.

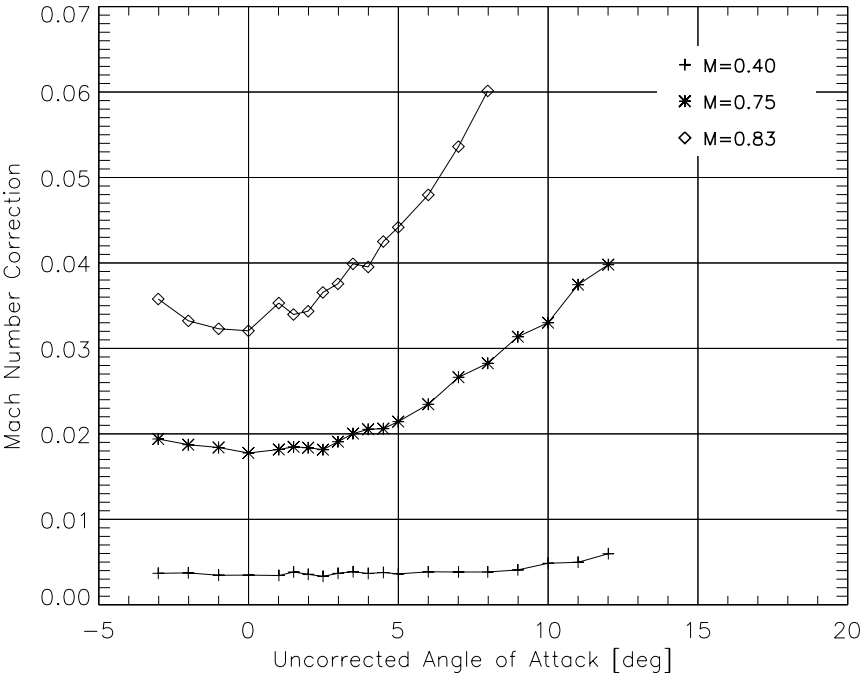

Figure 7(a). Mach number correction for closed wall configuration.

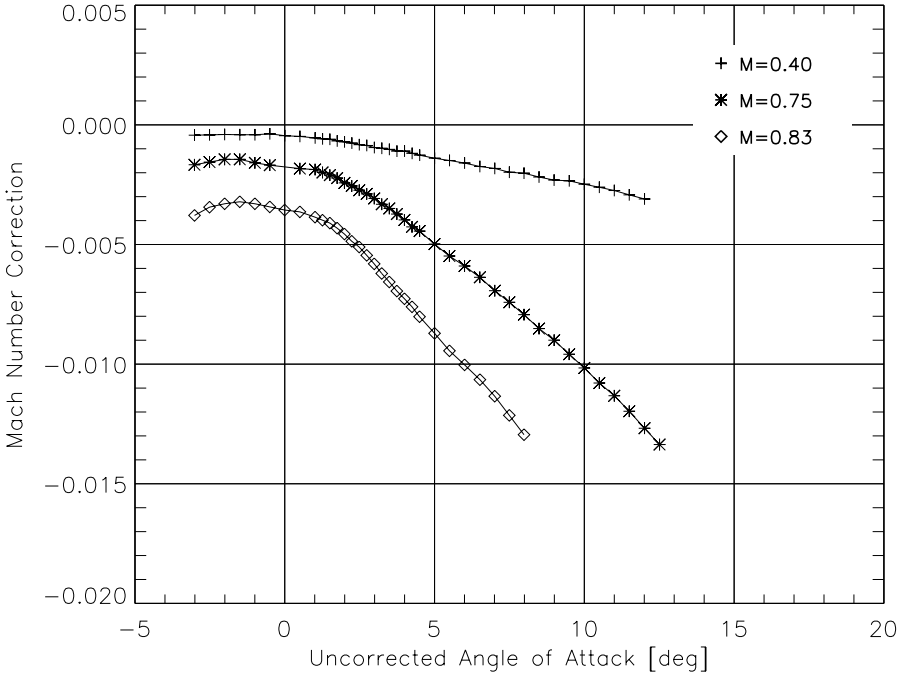

Figure 7(b). Mach number correction for slotted wall configuration.

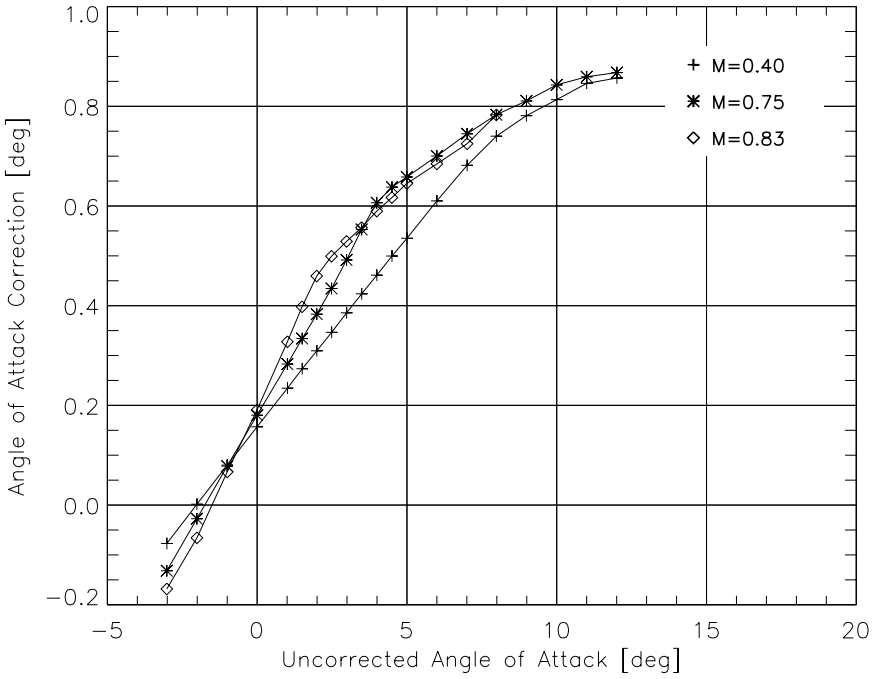

Figure 8(a). Angle of attack correction for closed wall configuration.

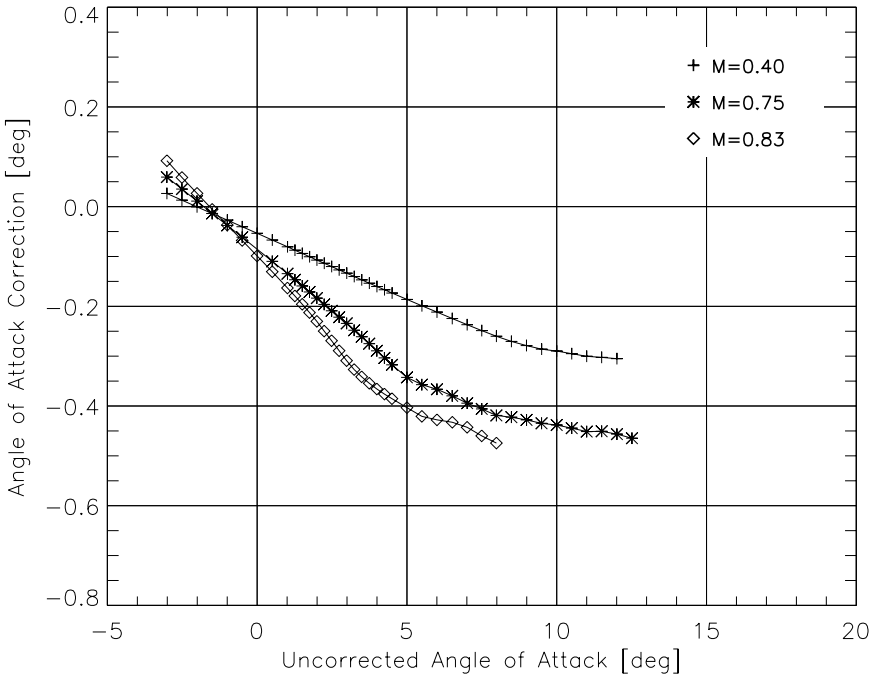

Figure 8(b). Angle of attack correction for slotted wall configuration.

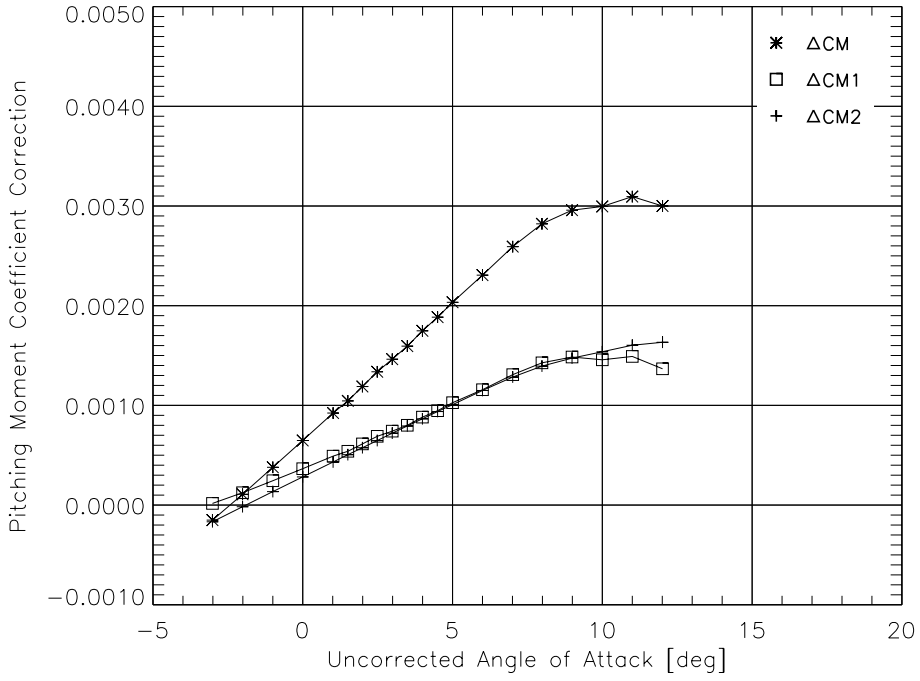

Figure 9(a). Pitching moment coefficient correction (closed wall conf., $M = 0.40$).

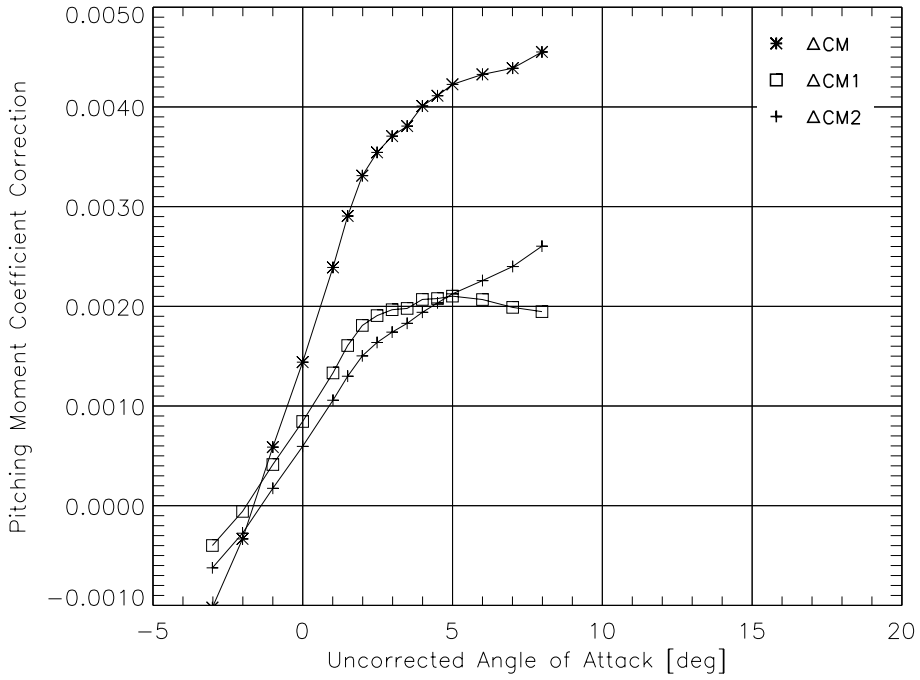

Figure 9(b). Pitching moment coefficient correction (closed wall conf., $M = 0.83$).

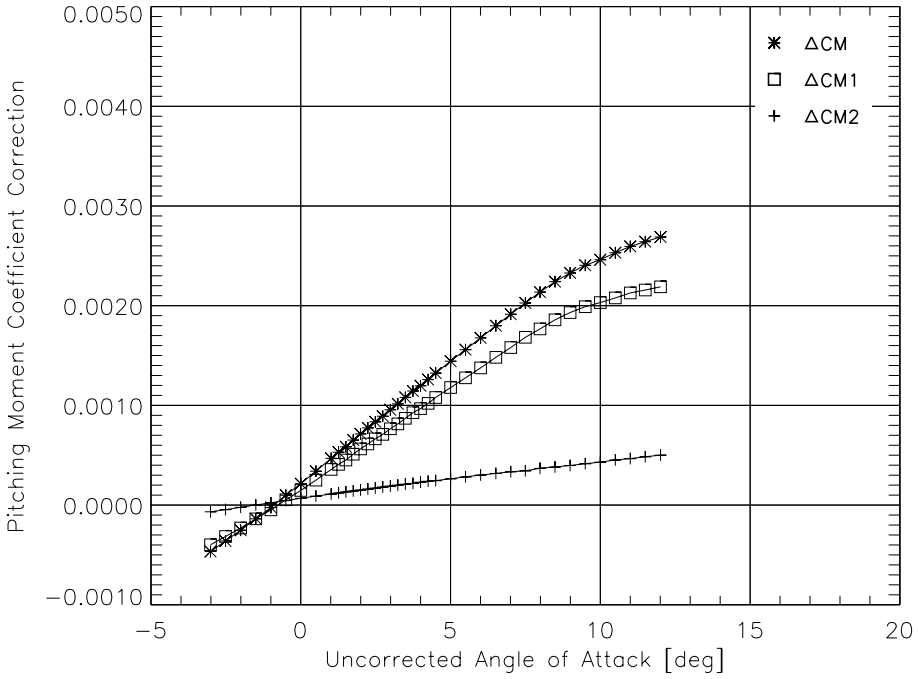

Figure 9(c). Pitching moment coefficient correction (slotted wall conf., $M = 0.40$).

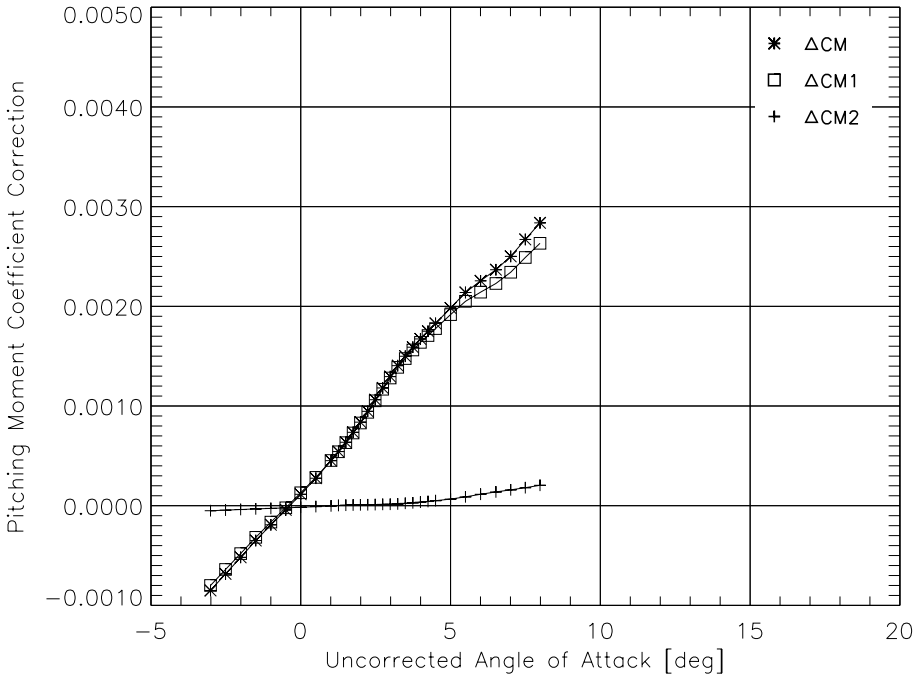

Figure 9(d). Pitching moment coefficient correction (slotted wall conf., $M = 0.83$).

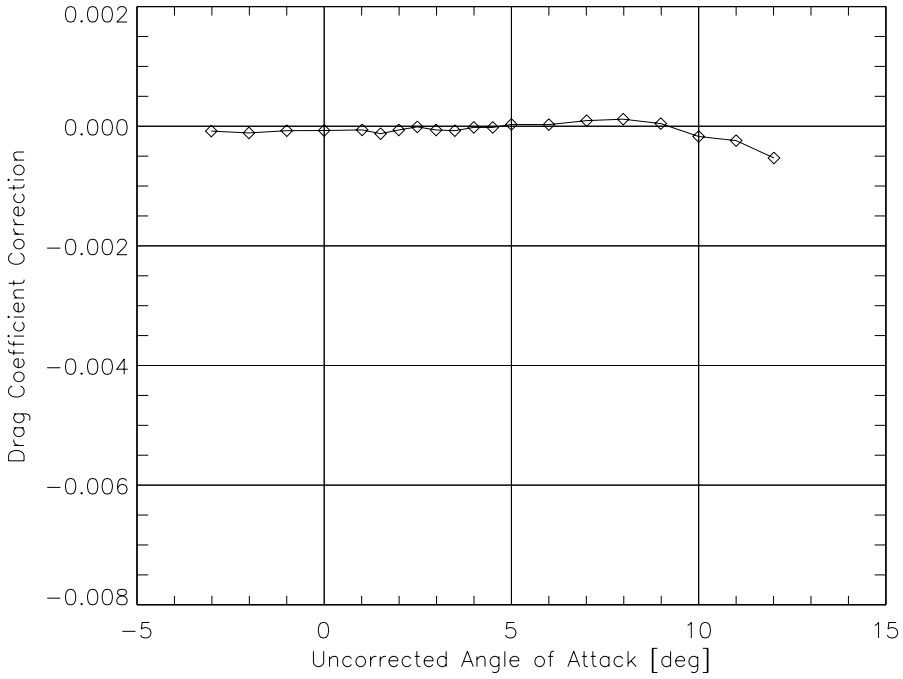

Figure 10(a). Wall interference induced buoyancy correction (closed wall conf., $M = 0.40$).

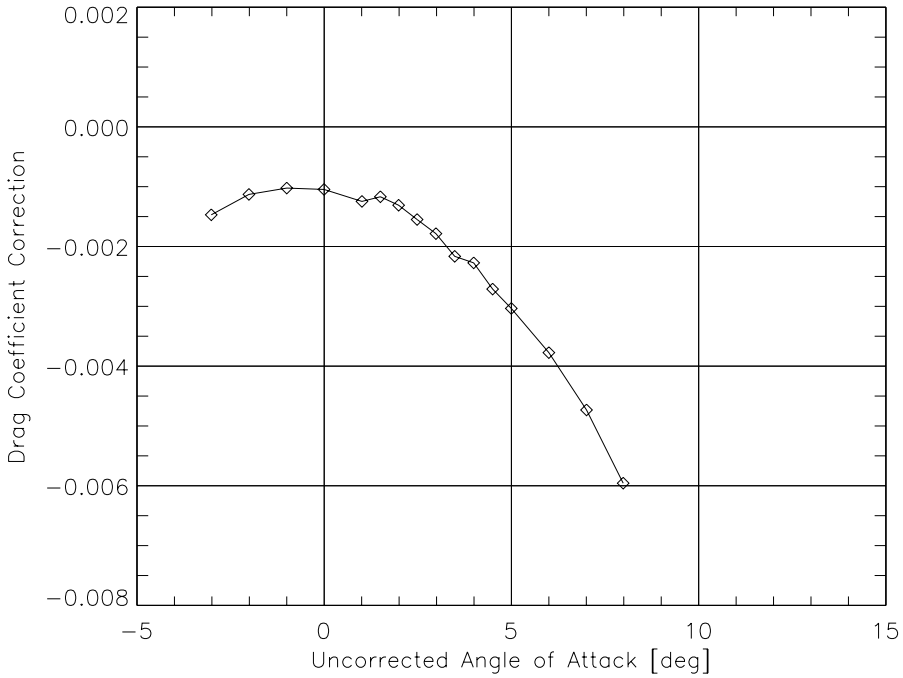

Figure 10(b). Wall interference induced buoyancy correction (closed wall conf., $M = 0.83$).

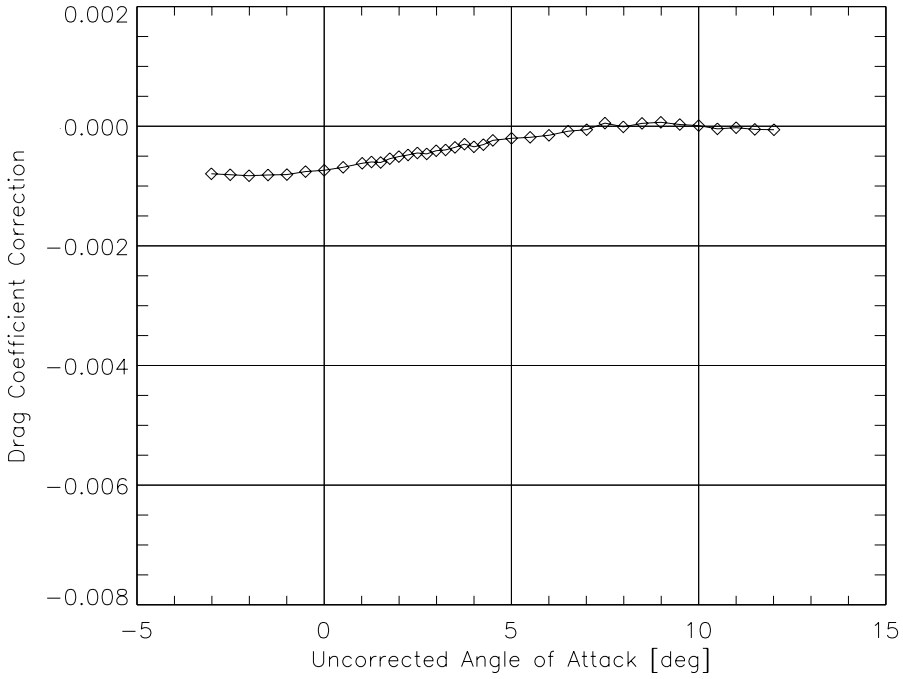

Figure 10(c). Wall interference induced buoyancy correction (slotted wall conf., $M = 0.40$).

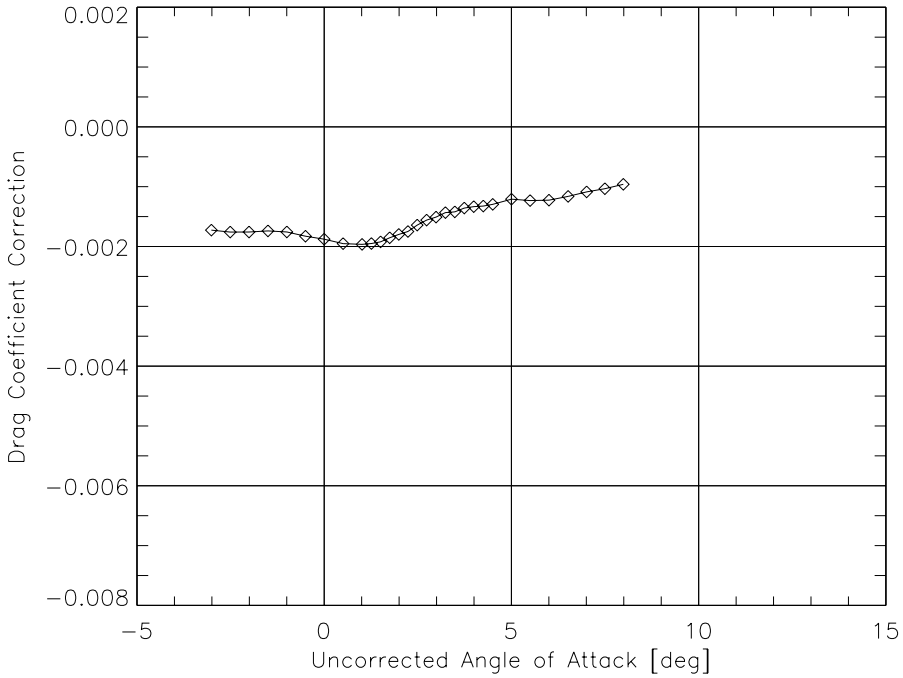

Figure 10(d). Wall interference induced buoyancy correction (slotted wall conf., $M = 0.83$).

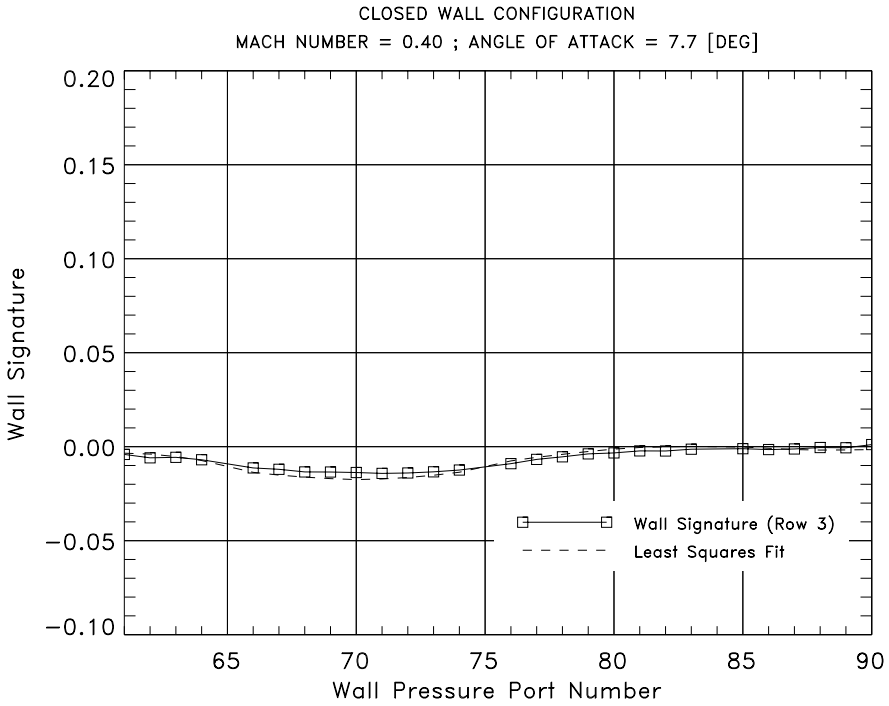

Figure 11(a). Wall signature on wall pressure port row 3 (closed wall conf., $M = 0.40$).

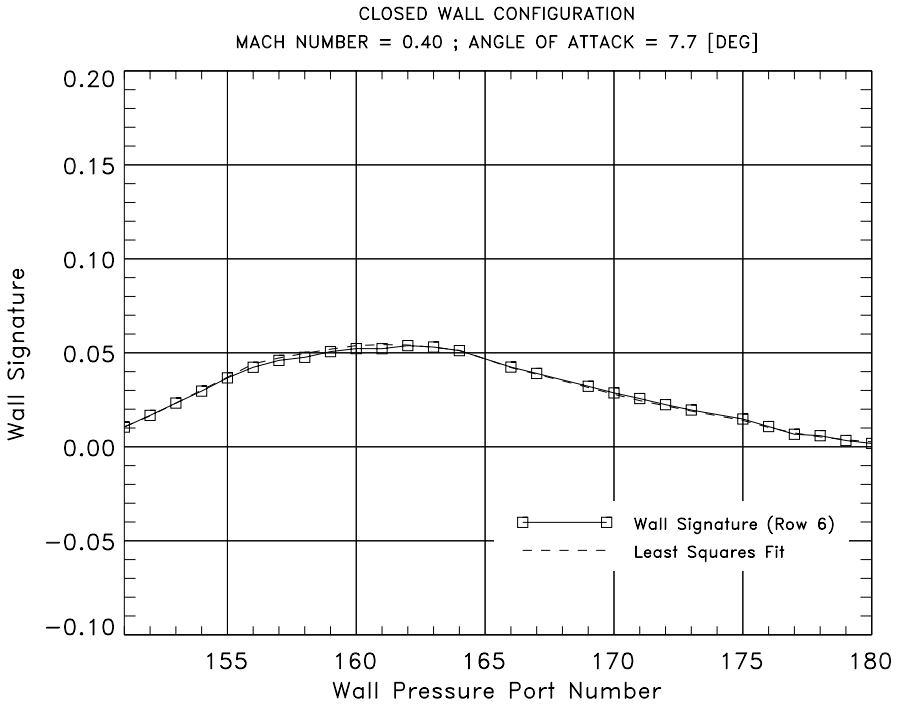

Figure 11(b). Wall signature on wall pressure port row 6 (closed wall conf., $M = 0.40$).

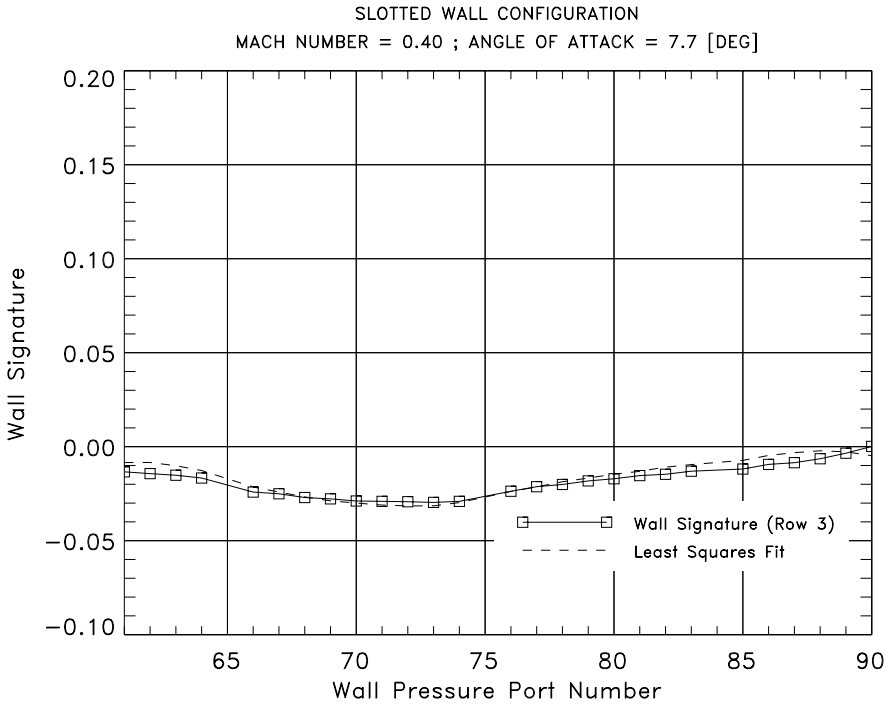

Figure 11(c). Wall signature on wall pressure port row 3 (slotted wall conf., $M = 0.40$).

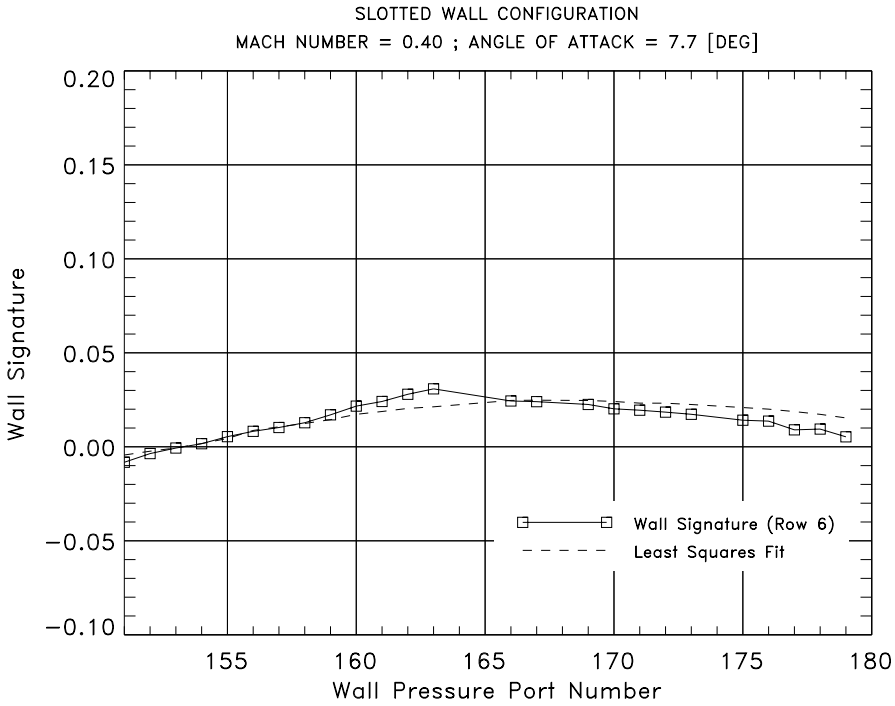

Figure 11(d). Wall signature on wall pressure port row 6 (slotted wall conf., $M = 0.40$).

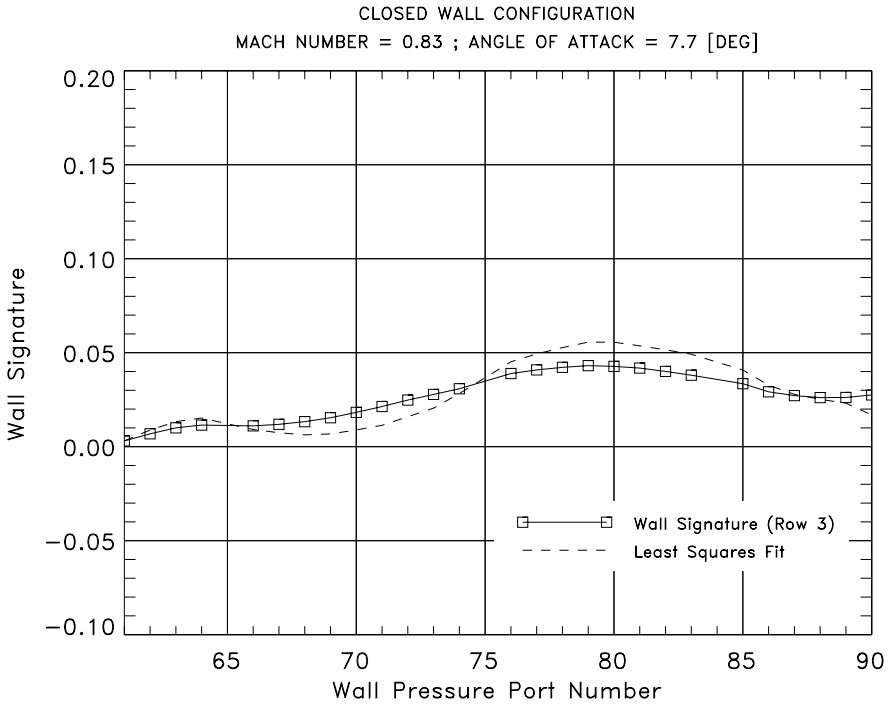

Figure 11(e). Wall signature on wall pressure port row 3 (closed wall conf., $M = 0.83$).

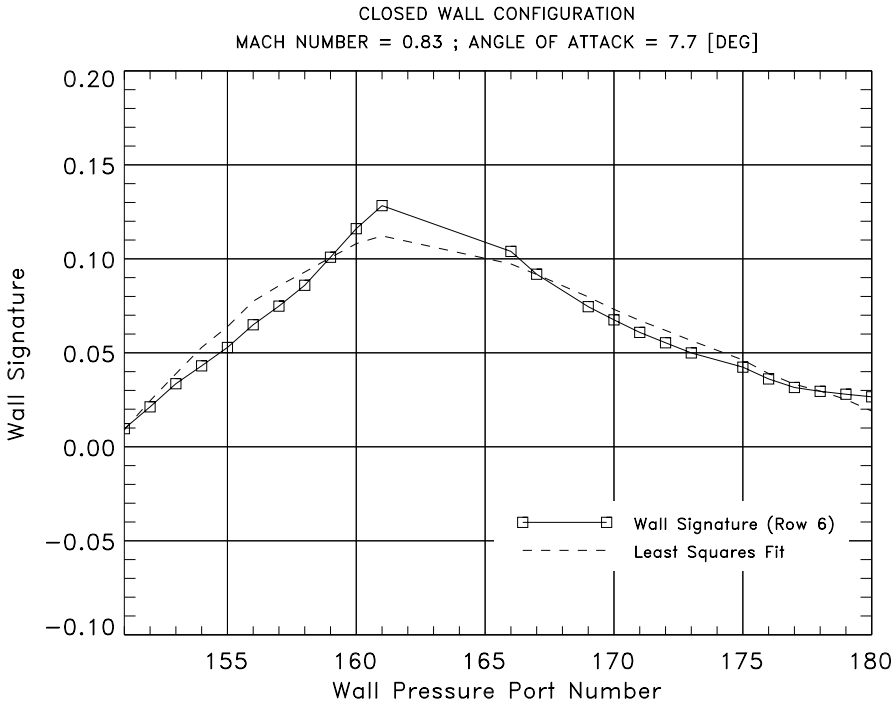

Figure 11(f). Wall signature on wall pressure port row 6 (closed wall conf., $M = 0.83$).

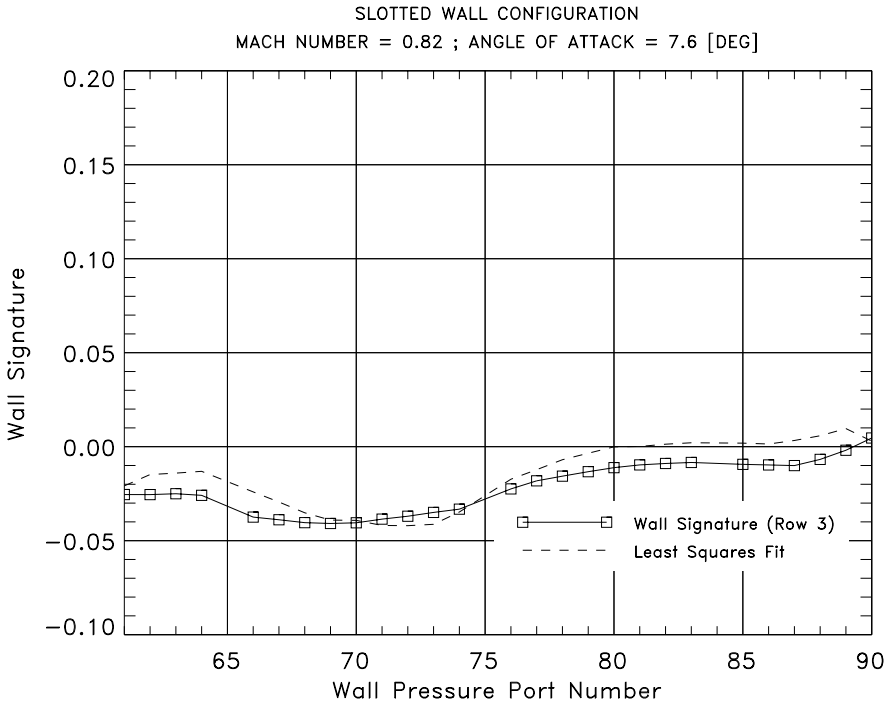

Figure 11(g). Wall signature on wall pressure port row 3 (slotted wall conf., $M = 0.82$).

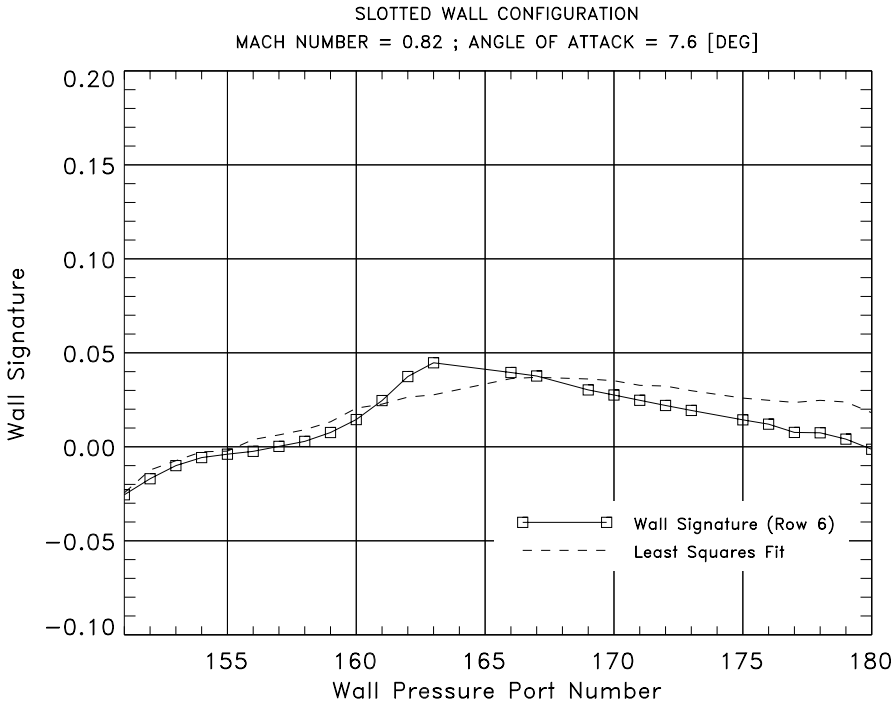

Figure 11(h). Wall signature on wall pressure port row 6 (slotted wall conf., $M = 0.82$).

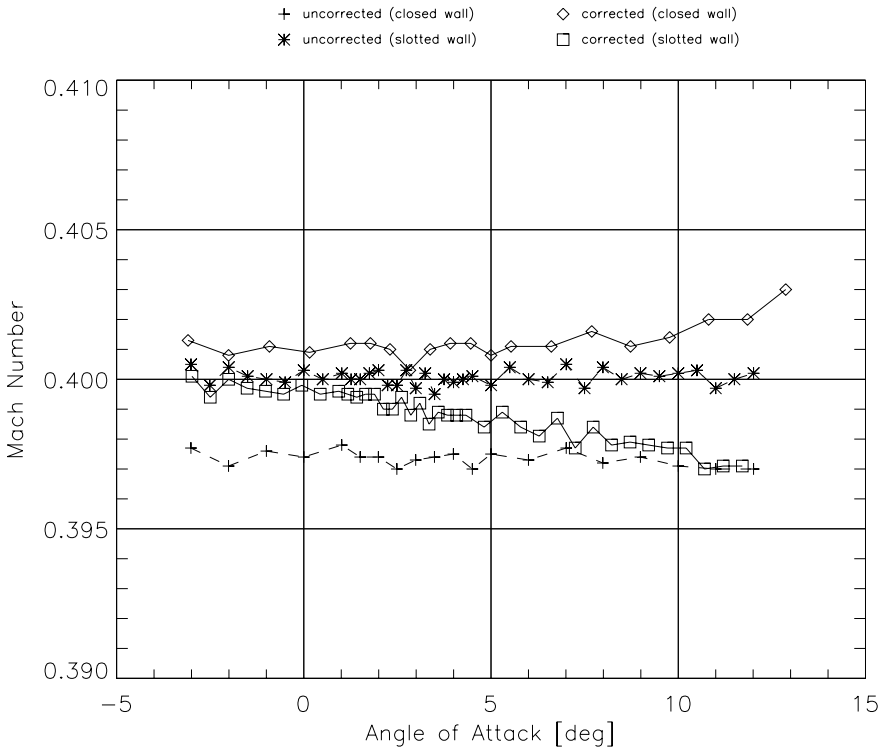

Figure 12(a). Uncorrected and corrected Mach number (target Mach number 0.40).

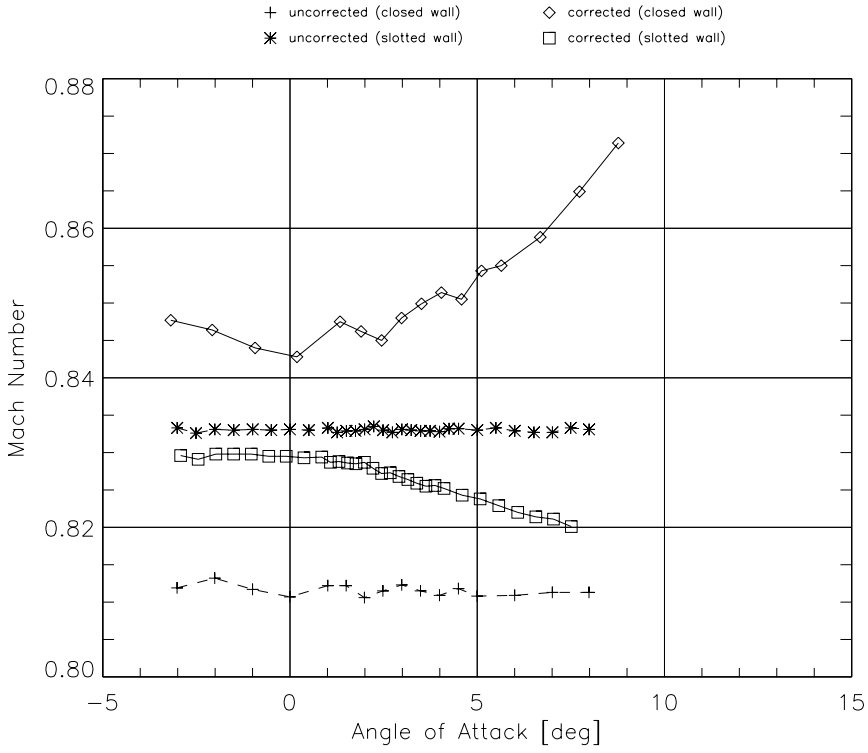

Figure 12(b). Uncorrected and corrected Mach number (target Mach number 0.83).

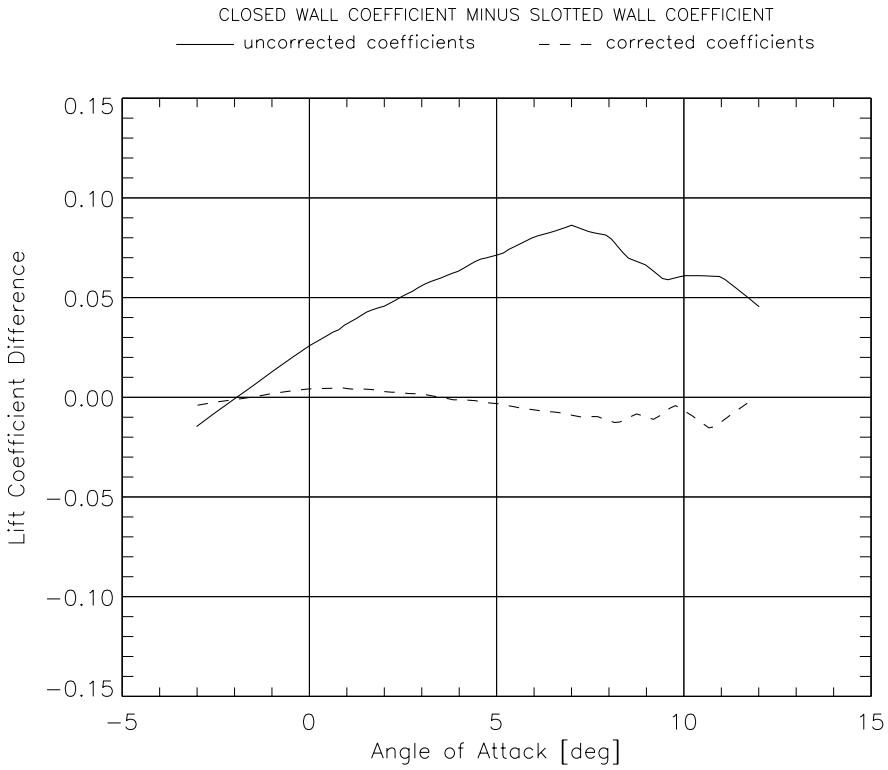

Figure 13(a). Lift coefficient differences ($M = 0.40$).

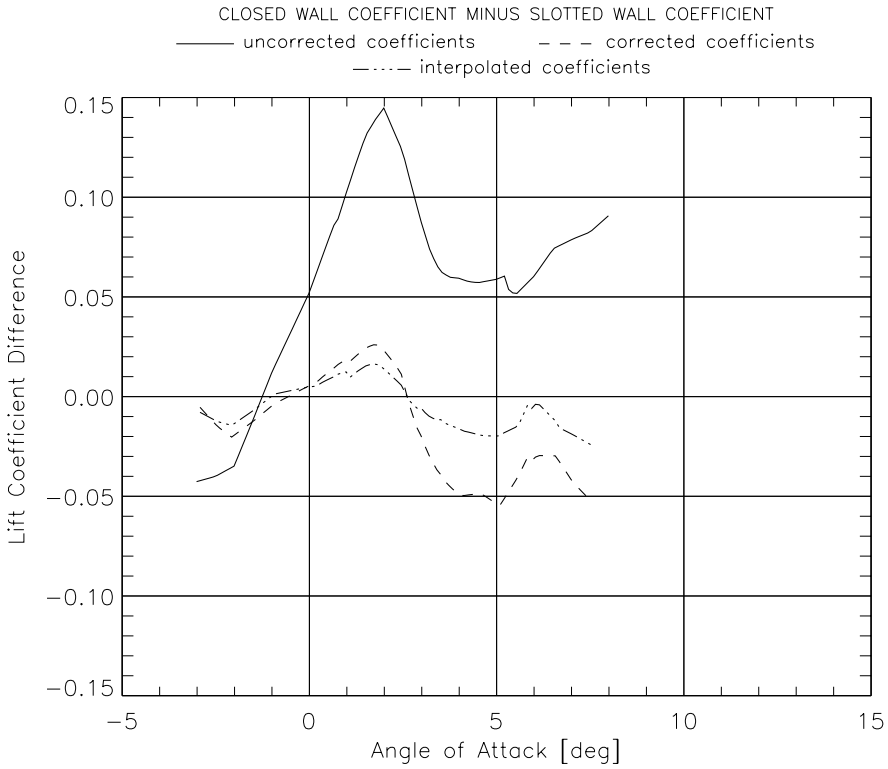

Figure 13(b). Lift coefficient differences ($M = 0.83$).

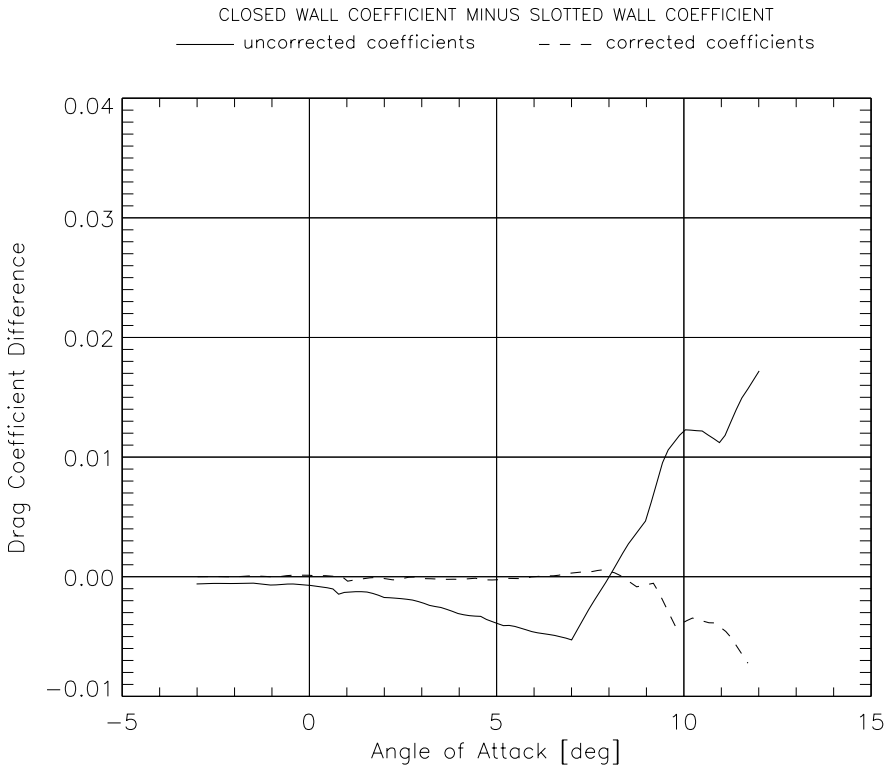

Figure 14(a). Drag coefficient differences ($M = 0.40$).

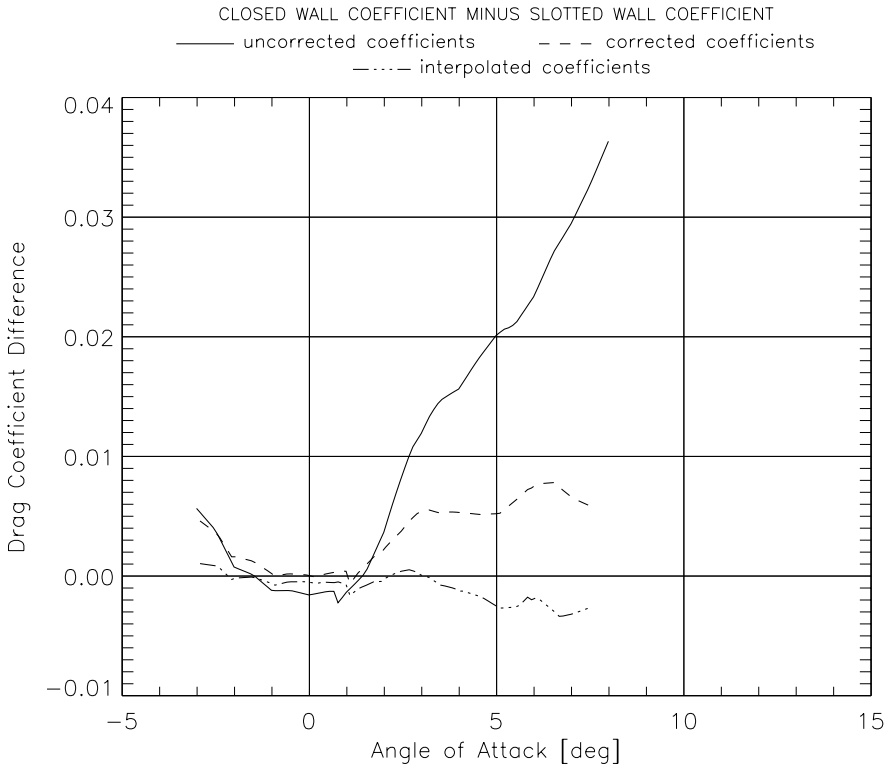

Figure 14(b). Drag coefficient differences ($M = 0.83$).

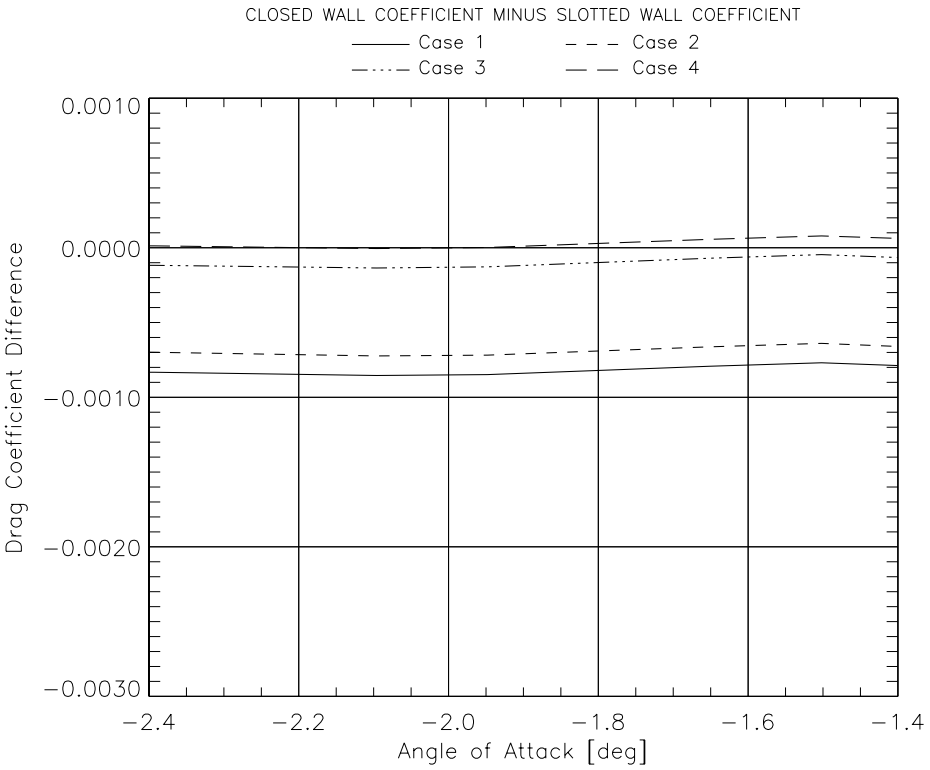

Figure 15(a). Influence of buoyancy corrections on drag coefficient differences ($M = 0.40$).

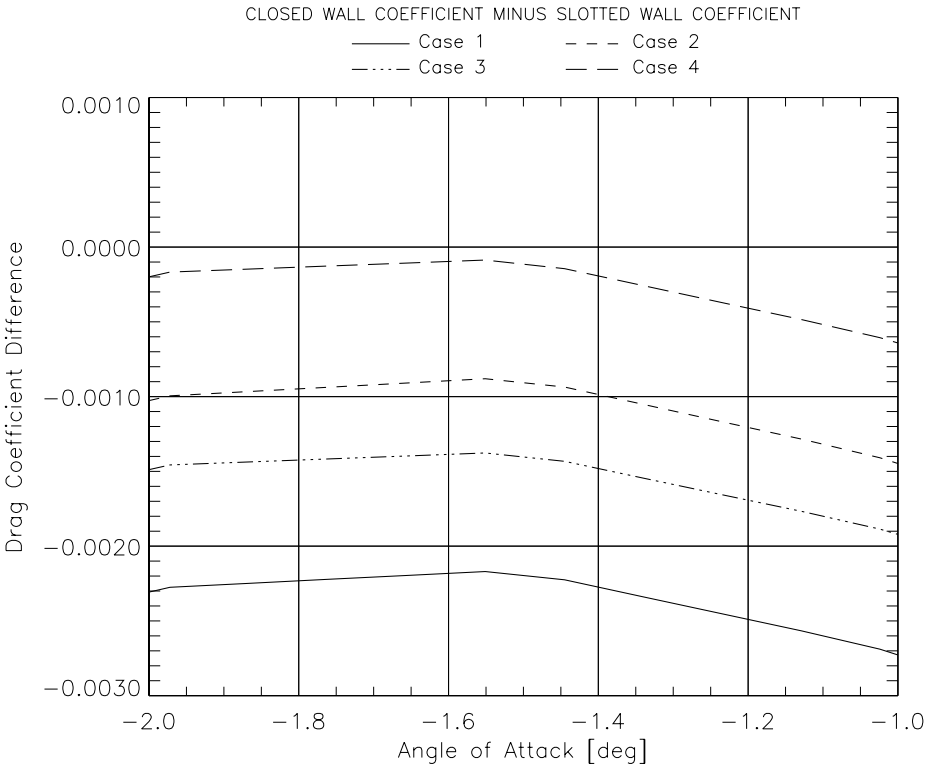

Figure 15(b). Influence of buoyancy corrections on drag coefficient differences ($M = 0.83$).

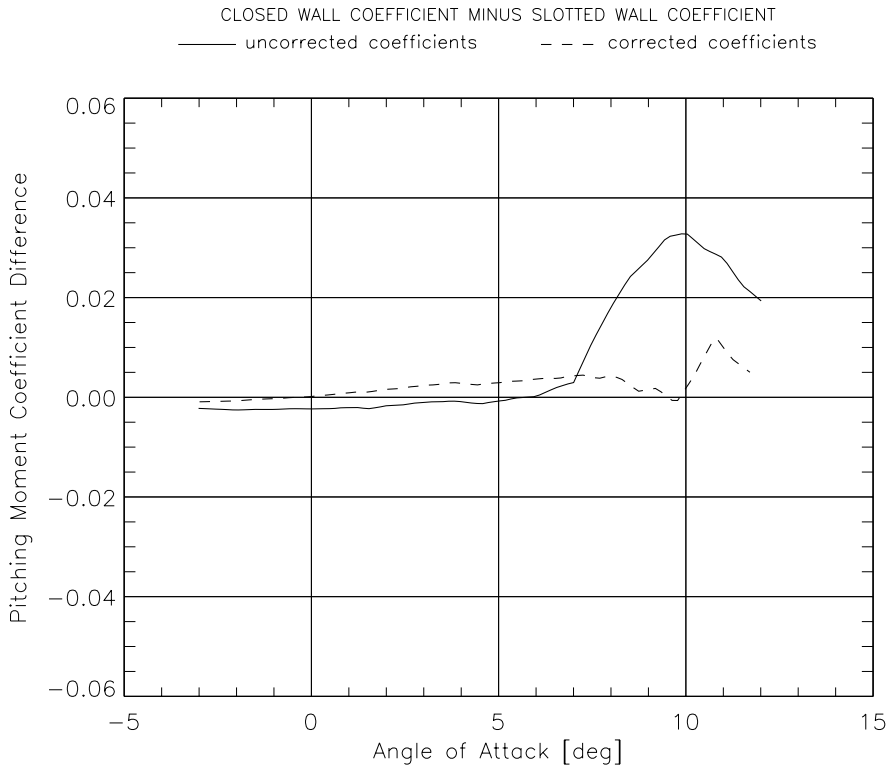

Figure 16(a). Pitching moment coefficient differences ($M = 0.40$).

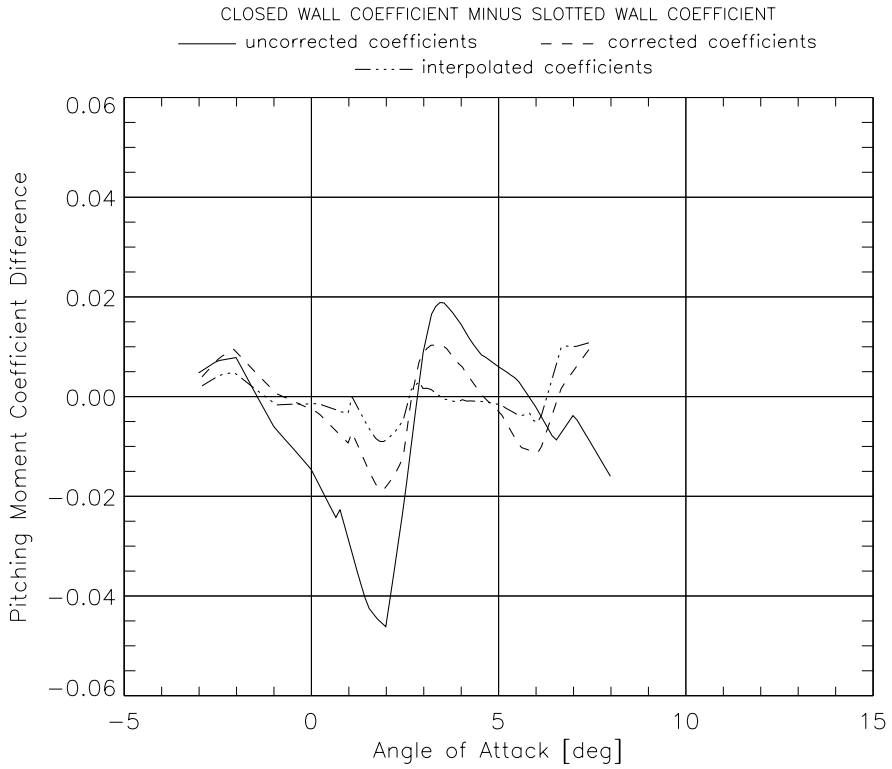

Figure 16(b). Pitching moment coefficient differences ($M = 0.83$).

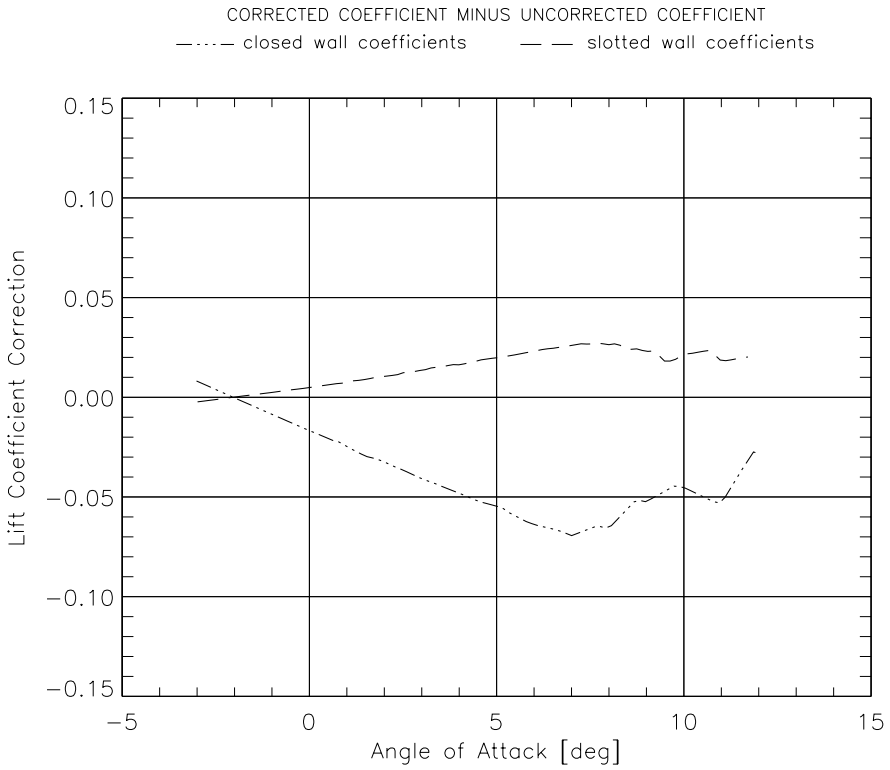

Figure 17(a). Total lift coefficient correction ($M = 0.40$).

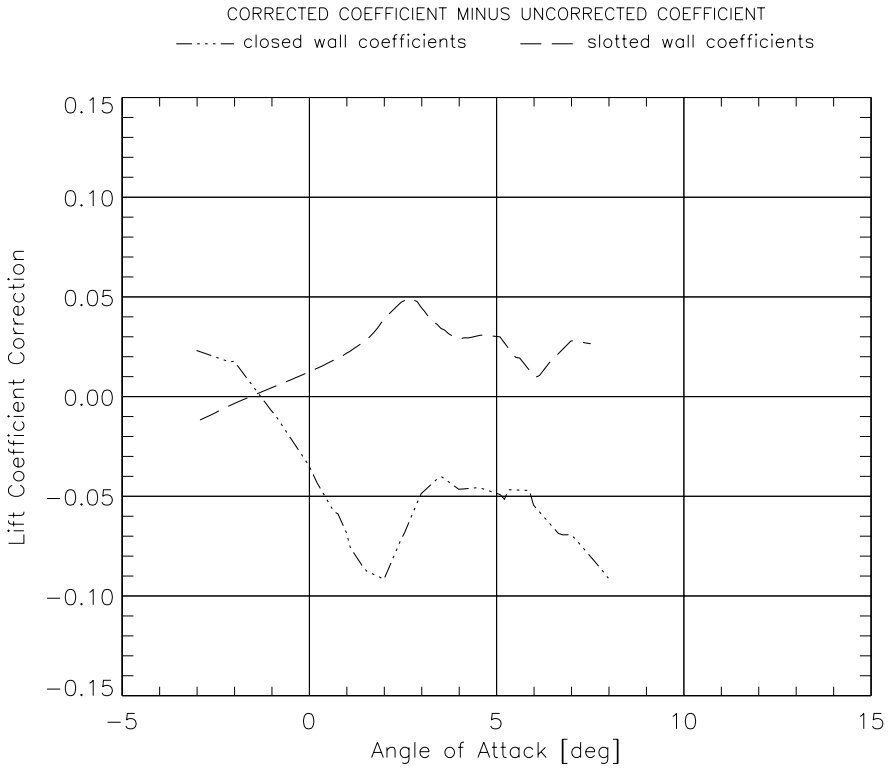

Figure 17(b). Total lift coefficient correction ($M = 0.83$).

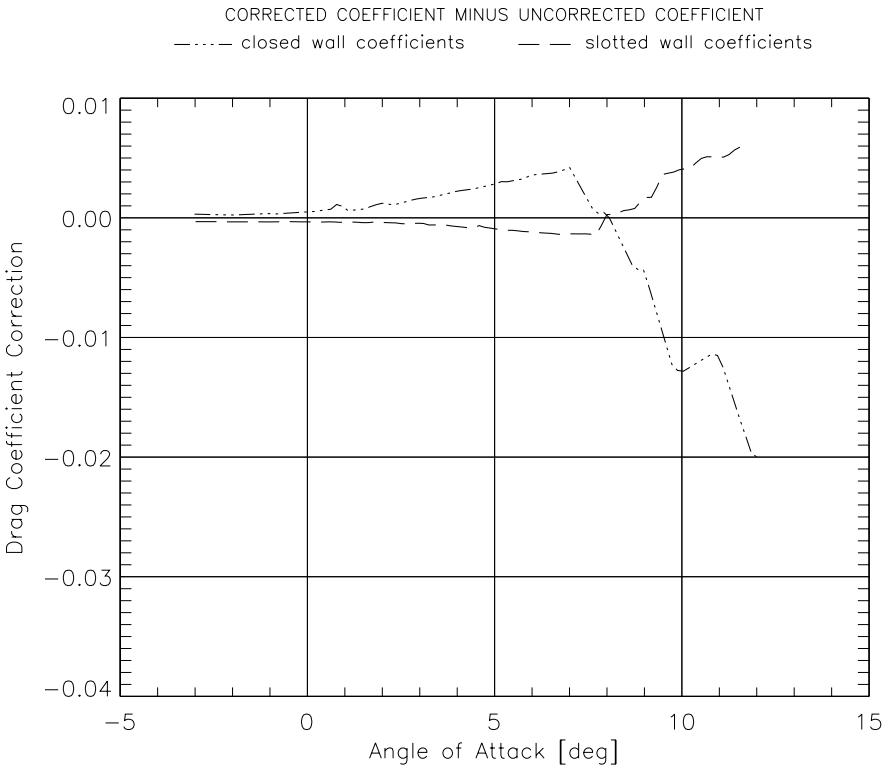

Figure 18(a). Total drag coefficient correction ($M = 0.40$).

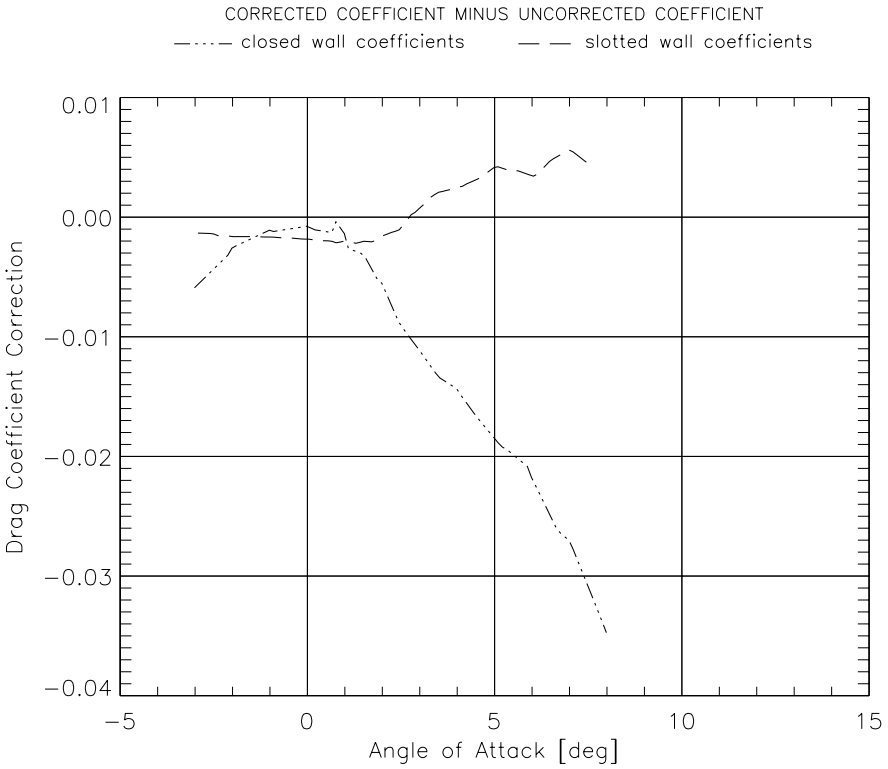

Figure 18(b). Total drag coefficient correction ($M = 0.83$).

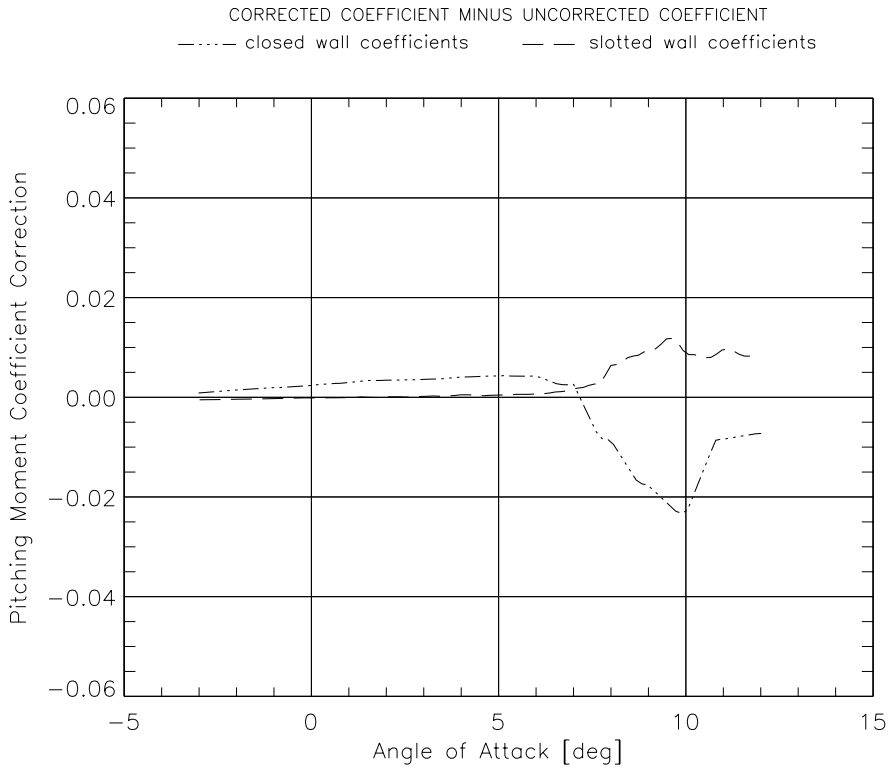

Figure 19(a). Total pitching moment coefficient correction ($M = 0.40$).

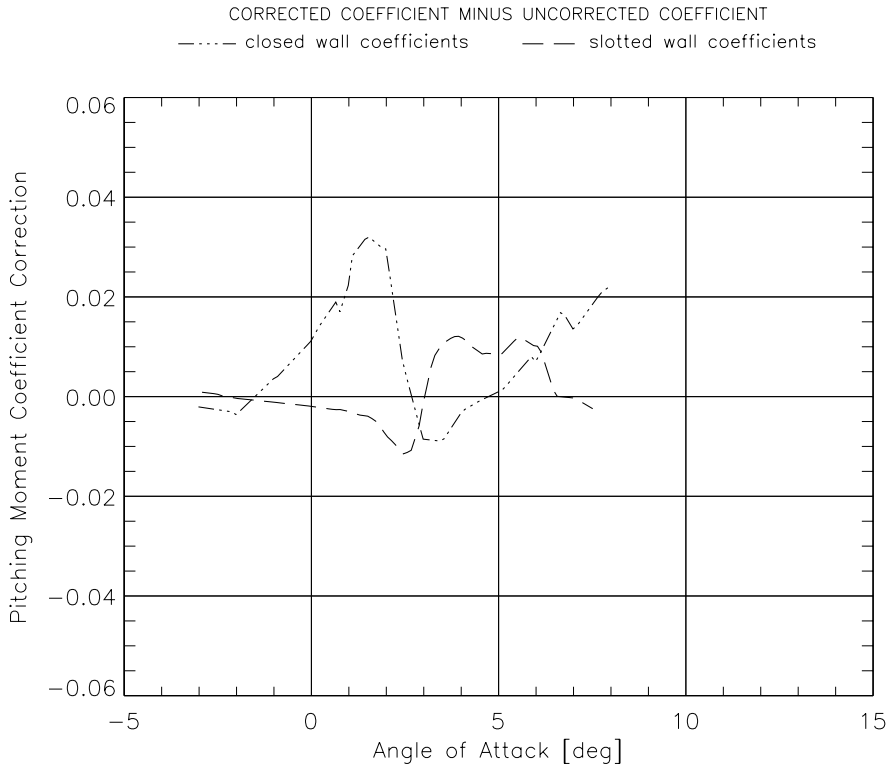

Figure 19(b). Total pitching moment coefficient correction ($M = 0.83$).

REPORT DOCUMENTATION PAGE

Form Approved
OMB No. 0704-0188

1. AGENCY USE ONLY *(Leave blank)*	2. REPORT DATE	3. REPORT TYPE AND DATES COVERED
	May 2003	Technical Memorandum

4. TITLE AND SUBTITLE

Direct Validation of the Wall Interference Correction System of the Ames 11-Foot Transonic Wind Tunnel

5. FUNDING NUMBERS

NAS 2-98083

6. AUTHOR(S)

Norbert Ulbrich, Alan R. Boone

7. PERFORMING ORGANIZATION NAME(S) AND ADDRESS(ES)

Sverdrup Technology, Inc., P.O. Box 366, M/S 227-4
Moffett Field, CA 94035-1000

Ames Research Center, Wind Tunnel Operations Division
Moffett Field, CA 94035-1000

8. PERFORMING ORGANIZATION REPORT NUMBER

A-03010210

9. SPONSORING/MONITORING AGENCY NAME(S) AND ADDRESS(ES)

National Aeronautics and Space Administration
Washington, DC 20546-0001

10. SPONSORING/MONITORING AGENCY REPORT NUMBER

NASA/TM–2003-212268

11. SUPPLEMENTARY NOTES

Point of Contact: Norbert Ulbrich, Ames Research Center, MS 227-5, Moffett Field, CA 94035-1000
(650) 604-6893

12a. DISTRIBUTION/AVAILABILITY STATEMENT

Unclassified — Unlimited
Subject Category 09 Distribution: Standard
Availability: NASA CASI (301) 621-0390

12b. DISTRIBUTION CODE

13. ABSTRACT ***(Maximum 200 words)***

Data from the test of a large semispan model was used to perform a direct validation of a wall interference correction system for a transonic slotted wall wind tunnel. At first, different sets of uncorrected aerodynamic coefficients were generated by physically changing the boundary condition of the test section walls. Then, wall interference corrections were computed and applied to all data points. Finally, an interpolation of the corrected aerodynamic coefficients was performed. This interpolation made sure that the corrected Mach number of a given run would be constant. Overall, the agreement between corresponding interpolated lift, drag, and pitching moment coefficient sets was very good. Buoyancy corrections were also investigated. These studies showed that the accuracy goal of one drag count may only be achieved if reliable estimates of the wall interference induced buoyancy correction are available during a test.

14. SUBJECT TERMS

transonic wind tunnel, wall interference corrections, correction validation

15. NUMBER OF PAGES

62

16. PRICE CODE

A04

17. SECURITY CLASSIFICATION OF REPORT	18. SECURITY CLASSIFICATION OF THIS PAGE	19. SECURITY CLASSIFICATION OF ABSTRACT	20. LIMITATION OF ABSTRACT
Unclassified	Unclassified		